**PEOPLE'S DEMOCRATIC REPUBLIC OF ALGERIA**
**MINISTRY OF HIGHER EDUCATION AND SCIENTIFIC RESEARCH**
**UNIVERSITY OF MSILA**

FACULTY: **Science**
DEPARTMENT: **Chemistry**
N°:……..……..

DOMAIN: **Material Science**

OPTION: **Composite Material and the environment**

**Thesis presented for the award of**

**Doctor of Philosophy**

**by**

**SAOUDI Ahmed**

**Title**

# Study of a quaternary material of the type $Cu_2ZnSnS_4$ used in solar cells

Committee in charge:

| Name and Surname | Grade | University | Role |
|---|---|---|---|
| **Debih Elhadi** | **Prof.** | **University of M'sila** | **President** |
| **Bouznit Yazid** | **Prof.** | **University of M'sila** | **Reporter** |
| **Noufel Kamel** | **MCA.** | **University of M'sila** | **Examiner** |
| **Mahmoudia Nabil** | **Prof.** | **University of JIJEL** | **Examiner** |

Copyright © SAOUDI Ahmed, 2026

All rights reserved

# Acknowledgments

*This study was conducted within the Chemistry Laboratory at the University of M'sila, under the supervision of Professor* ***Bouznit Yazid****.*

*I wish to express my deepest gratitude to my professor* ***Bouznit Yazid*** *for his invaluable role as my advisor. His unwavering availability, insightful guidance, and attentive support were instrumental, providing both scientific expertise and moral encouragement throughout the process.*

*I also extend my profound thanks to Mr.* ***Noufel Kamel*** *from the University of M'sila. May he find in these words the expression of my boundless appreciation, particularly for graciously agreeing to serve as an examiner on the thesis defense jury.*

*Similarly, I offer my deepest gratitude to Mr.* **Mahmoudia Nabil** *from the University of Jijel for kindly accepting the role of examiner on the defense jury.*

*It is with great pleasure that I convey my sincere thanks to Mr* ***Debih Elhadi*** *from the University of M'sila for agreeing to chair the jury.*

# Dedication

I dedicate this work to:

My beloved parents,

whose love and sacrifices have guided me throughout this journey. No words can adequately express the gratitude and affection I hold for them.

To my entire family,

for their constant presence, unwavering support, and precious love. Please accept here the expression of my deepest gratitude.

**TABLE OF CONTENTS**

VITA

2014 Bachelor of Science in Pharmaceutical Chemistry, University of Msila

2016 Master of Science in Organic Chemistry, University of Msila

2026 PhD in Composite Materials and Environmental Science, University of M'sila

**PUBLICATIONS**

1. **Dual effect to improve the electrical properties of SZO films grown by nitrogen pneumatic spray pyrolysis** (**DOI**:10.1002/jemt.24475)
2. **Substrate Effect On Photoelectrochemicel And Semicondictrise Properties Of Lead Oxide In 0.5 M H2SO4** (**DOI**:10.54966/jreen.v27i2.1155)
3. **Novel multi-spray approach for preparing $Cu_2ZnSnS_4$ films for efficient solar photoelectrochemical water splitting** (DOI: 10.1016/j.chemphys.2025.112894)

ABSTRACT OF THE DISSERTATION

A novel multi-spray approach was developed and optimized for preparing high-quality $Cu_2ZnSnS_4$ (CZTS) thin films. Films prepared using this method were systematically compared with those deposited by conventional spray techniques in terms of surface morphology, crystal structure, and photoelectrochemical properties. To determine optimal deposition conditions, films with varying Cu:Zn:Sn:S atomic ratios were investigated. X-ray diffraction (XRD) revealed that phase formation strongly depended on these ratios. Single-phase CZTS films with a preferential (112) orientation were consistently obtained at the stoichiometric ratio (Cu:Zn:Sn:S = 2:1:1:4). All films exhibited relatively high optical transmittance (~50%) in the visible region. Furthermore, comprehensive structural, morphological, and electrochemical characterizations are detailed herein.

**Keywords:** Multi-spray approach; Thin films; $Cu_2ZnSnS_4$; Atomic ratio optimization.

**ملخص الأطروحة**

تم تطوير وتحسين طريقة رش متعددة جديدة لتحضير أغشية رقيقة عالية الجودة من مادة كبريت النحاس والزنك والقصدير $Cu_2ZnSnS_4$ (CZTS). تمت مقارنة الأغشية المحضرة بهذه الطريقة بشكل منهجي مع الأغشية المحضرة بالطريقة التقليدية من حيث البنية السطحية (المورفولوجيا)، والبنية البلورية، والخصائص الكهروضوئية. ولتحديد الظروف المثلى للترسيب، تم دراسة سلسلة من الأغشية بنسب ذرية مختلفة للعناصر (النحاس: الزنك: القصدير: الكبريت).

أظهرت نتائج حيود الأشعة السينية (XRD) أن تكوين الأطوار البلورية يعتمد بشكل كبير على هذه النسب الذرية. وتم الحصول باستمرار على أغشية CZTS أحادية الطور ذات توجه بلوري مفضل على المستوى (112)، وذلك عند استخدام النسبة الذرية المثلى (Cu:Zn:Sn:S = 2:1:1:4). كما أظهرت جميع الأغشية نفاذية بصرية عالية نسبياً بلغت حوالي 50% في منطقة الضوء المرئي. وتتناول هذه الدراسة بالتفصيل التوصيف الشامل للبنية البلورية، والتركيب السطحي، والخصائص الكهروكيميائية للأغشية المحضرة.

**الكلمات المفتاحية:** طريقة الرش المتعدد؛ أغشية رقيقة؛$Cu_2ZnSnS_4$ ؛ تحسين النسب الذرية.

# *GENERAL INTRODUCTION*

## General introduction

The escalating global energy demand, coupled with the need for sustainable and environmentally benign solutions, has accelerated research into renewable technologies, particularly photovoltaics (PV) [2]. Thin-film photovoltaics (TFPV) represent a compelling alternative to conventional silicon-based solar cells, offering reduced material usage, lower manufacturing costs, and greater flexibility in applications [3], [4]. Among TFPV absorbers, $Cu_2ZnSnS_4$ (CZTS) is particularly promising due to its direct bandgap of approximately 1.5 eV, high absorption coefficient exceeding $10^4$ $cm^{-1}$, and the earth-abundance and low toxicity of its elements—copper (Cu), zinc (Zn), tin (Sn), and sulfur (S)[5].

CZTS adopts a kesterite crystal structure (a tetragonal derivative of chalcopyrite), which facilitates efficient charge carrier transport and minimizes recombination losses. Its tunable bandgap and strong optical absorption also render it suitable for tandem solar cell architectures, broadening its utility in renewable energy systems [6]. However, realizing CZTS's full potential is impeded by challenges in maintaining stoichiometric accuracy, ensuring phase purity, and achieving uniform film morphology issues that often lead to secondary phases and defects, compromising device efficiency [2].

Conventional deposition techniques, such as sputtering and chemical vapor deposition (CVD), are limited by high processing temperatures, complex equipment requirements, and challenges in scalability[5],[7]. These drawbacks exacerbate problems like secondary phase formation (e.g., CuS or ZnS) and grain inhomogeneity, introducing defect states that degrade performance in photovoltaic and photoelectrochemical (PEC) water-splitting devices [8]. To overcome these barriers, innovative, cost-effective methods are imperative for producing high-quality CZTS films at scale, with applications spanning PV and PEC hydrogen production.

Spray deposition emerges as a viable solution, involving the atomization of precursor solutions into droplets that are directed onto heated substrates to form uniform thin films. This technique enhances scalability and substrate adaptability while maintaining low costs [9]. Spray pyrolysis, in particular, has proven effective in enhancing CZTS crystallinity, phase purity, and compositional control, with its simplicity and compatibility for large-area or flexible substrates

making it ideal for TFPV and PEC applications [7].

Recent innovations in spray technology, such as real-time process monitoring, rapid thermal annealing, and sulfurization treatments—have yielded CZTS films with optimized properties, including a 1.5 eV direct bandgap and elevated carrier concentrations for superior PV and PEC performance [7], [9]. This thesis advances this field by developing and optimizing a novel multi-spray deposition method for CZTS thin films, where precursors are mixed in the vapor phase for improved homogeneity. This approach systematically addresses stoichiometric challenges, compares multi-spray films to conventional ones in terms of morphology, structure, and PEC properties, and emphasizes CZTS's role in sustainable PV and water splitting.

The thesis is structured as follows:

Introduction: Outlines the research background, problem statement, significance, objectives, and scope. Chapter 1: Background and Fundamentals of CZTS Research: Discusses the economic, environmental, and scientific drivers for CZTS research, including essential material properties and photovoltaic applications. Chapter 2: State-of-the-Art Spray Deposition Techniques: Reviews designs, performance metrics, and recent advancements in spray-based CZTS fabrication.

Chapter 3: Experimental Techniques: Describes materials, deposition setup, parameters, post-treatments, and characterization methods. Chapter 4: Results and Discussion: Presents experimental data, analyzes findings, and optimizes deposition parameters. Conclusion: Summarizes key outcomes, implications, and future directions.

# *CHAPTER 1: BACKGROUND AND FUNDAMENTALS OF CZTS RESEARCH*

**Introduction**

Copper zinc tin sulfide (CZTS), chemically represented as $Cu_2ZnSnS_4$, is a quaternary chalcogenide semiconductor that has emerged as a promising material for sustainable energy applications due to its earth-abundant composition and non-toxic elements, contrasting with cadmium telluride (CdTe) or copper indium gallium selenide (CIGS) which rely on rare or hazardous materials as highlighted in reviews emphasizing CZTS for low-cost PV [2]. Its direct band gap of 1.4–1.6 eV aligns well with the solar spectrum, enabling efficient photon absorption, while its high absorption coefficient exceeding $10^4$ $cm^{-1}$ allows for thin-film configurations that reduce material consumption confirmed in studies on CZTS luminescence and defects[10] . CZTS thin films can be synthesized through various techniques, including physical vapor deposition methods like sputtering and thermal evaporation, which offer precise control but require high vacuum and energy inputs, making them less scalable for industrial production. In contrast, solution-based methods such as electrodeposition and sol-gel provide low-cost alternatives but often suffer from uniformity issues and the need for post-annealing to achieve crystallinity. Among these, spray pyrolysis stands out for its versatility, involving the atomization of precursor solutions (typically containing copper, zinc, tin, and sulfur sources like thiourea) into fine droplets that decompose on heated substrates, forming uniform films at atmospheric pressure as demonstrated in ultrasonic spray for CZTS [11]. This method's advantages include rapid deposition rates, compatibility with large-area substrates, and tunable parameters like substrate temperature (300–450°C), spray rate, and precursor concentration, which influence film stoichiometry and phase purity optimized in Ge-alloyed CZTSe for 4.72% efficiency *[12]*. Recent studies have optimized spray pyrolysis by incorporating laser irradiation post-deposition to enhance crystallinity and reduce defects, leading to improved photovoltaic efficiencies with efficiencies up to 5.8% in Ag-containing CZTS [13]. However, literature gaps persist in exploring variants like field-assisted spray pyrolysis, which applies electric fields to direct aerosol particles, yielding orthorhombic CZTS with enhanced adhesion as noted in CZTS reviews *[14]*. Ultrasonic spray methods address uniformity by generating finer mists, resulting in nano-crystalline films with band gaps closer to 1.5 eV achieved at low temperatures. Nebulizer-assisted spray has been shown to produce stoichiometric CZTS without toxic sulfurization, minimizing environmental impact as in spray for CZTS [15]. Comparisons reveal that spray-deposited CZTS achieves efficiencies of 2–7% in solar cells, lagging behind hydrazine-processed CZTSSe (12.6%) due to recombination losses, but

surpassing electrodeposited films in cost-effectiveness – as reviewed [16]. Thermal treatments in spray processes, such as two-stage annealing, improve grain size and reduce secondary phases like $Cu_2SnS_3$ or ZnS, which are common defects – with improvements in CZTS from xanthate precursors [17]. This thesis bridges these gaps by focusing on spray optimization for CZTS, emphasizing precursor ratios and substrate effects to enhance optoelectronic performance – as in spray for Ge-alloyed CZTSe [18]. Emerging research integrates spray with doping (e.g., Ag or Ge) to tune properties, offering pathways for next-generation devices – achieving 5.8% with Ag [16]. Overall, CZTS's potential in photovoltaics underscores the need for scalable deposition like spray, with ongoing challenges in defect engineering – addressed in recent reviews [19]. Future directions include hybrid spray-vacuum approaches for higher efficiencies – as in CZTS synthesis [20]. This introduction sets the foundation for exploring CZTS properties and applications in subsequent sections.

## 1.1 Motivation and Research Scope

The motivation for this work stems from the combined economic, environmental, and scientific appeal of CZTS. Comprehensively studying spray pyrolysis parameters—precursor mixing, droplet formation, substrate preparation, temperature profiles, and subsequent annealing—can lead to new insights into how to produce uniform, high-purity films. Second, investigating a custom-built spray system allows one to eliminate many of the limitations found in commercial setups, such as fixed nozzle geometries or restrictive temperature ranges. Third, evaluating the synthesized films for solar device applications ensures that theoretical improvements translate into tangible performance gains. In the broader solar energy community, further progress in CZTS depends on surmounting persistent problems such as secondary-phase suppression, stoichiometric precision, and doping strategies that fine-tune electronic and optical properties. The homemade spray pyrolysis method presented here provides considerable flexibility in precisely reconfiguring a range of parameters pivotal to addressing these issues. By coupling the as-deposited films with thorough characterization (including Raman spectroscopy, XRD, SEM, and other elemental or optical measurements), this project aims to clarify the strategies that can sustainably improve the device-level performance of CZTS absorbers.

## 1.2 Concepts of Thin Films

Thin films are defined as material layers with thicknesses from a few nanometers to several micrometers, engineered to exhibit unique properties distinct from bulk counterparts due to surface effects, quantum confinement, and interfacial interactions as in CZTS synthesis. In CZTS contexts, thin films serve as absorbers in solar cells, where thickness optimization (typically 1–2 μm) balances light absorption and charge carrier diffusion lengths to minimize recombination [18]. Key concepts include nucleation and growth mechanisms, such as Volmer-Weber (island growth) or Frank-van der Merwe (layer-by-layer), influenced by substrate surface energy and deposition kinetics in spray methods [21]. Adhesion is critical, governed by van der Waals forces and chemical bonding; in spray pyrolysis, preheated substrates (e.g., glass or Mo-coated) enhance wetting and reduce peeling [22]. Uniformity ensures consistent optoelectronic performance, achieved in spray by controlling nozzle distance and carrier gas flow, contrasting with sputtering's line-of-sight limitations as compared in reviews [23] Phase stability involves avoiding polymorphic transitions; CZTS films must maintain kesterite phase to prevent band gap shifts [24]. Deposition parameters like temperature affect morphology: higher temperatures promote larger grains but risk volatilization of Sn or S – as in spray at low temps [22]. Precursor ratios (e.g., Cu-poor, Zn-rich) mitigate defects like Cu-Zn antisites, common in quaternary systems – confirmed in Ge-doping [23]. Compared to other methods, spray offers ambient processing, reducing energy costs by 50–70% versus vacuum techniques – from cost analyses [25]. Thin film defects, such as voids or pinholes, can be minimized via multi-layer spraying, improving density [26]. Optical interference in thin films affects measurements; CZTS films exhibit Fabry-Perot fringes in spectra – observed in luminescence [10]. Mechanical stress, arising from thermal expansion mismatches, impacts longevity; spray on flexible substrates like PET enables bendable devices – as in bifacial CZTSSe [10]. Scalability is a core concept, with spray enabling roll-to-roll processing for commercial viability – highlighted in reviews [14]. Environmental factors, like humidity during deposition, influence hydrolysis and film quality [16]. This section underscores thin films' role in CZTS technology, linking to properties discussed next. Future concepts involve nanostructured films for enhanced surface effects [17]. Integration with nanomaterials could further refine these principles.

## 1.3 Properties of CZTS

CZTS thin films display multifaceted properties tunable by deposition techniques, with spray methods enabling defect control and phase selectivity for optimized performance – as in spray CZTS [27]. As a direct bandgap p-type semiconductor, CZTS inherently shows hole-dominated conduction, with properties influenced by intrinsic defects like Cu vacancies – evident in defect studies [28]. Polymorphism between kesterite and stannite structures affects stability, with kesterite being thermodynamically preferred – as in CZTS synthesis [19]. Spray deposition influences these via substrate temperature, yielding films with reduced Cu/Zn disorder compared to sol-gel [20]. Band tailing due to disorder impacts efficiency, a common issue in quaternary chalcogenides – as reviewed [29]. Doping with Ag mitigates this, enhancing overall properties – achieving 5.8% efficiency [30]. Comparisons show spray CZTS has crystallinity akin to evaporated films but at lower costs – from Ge-doping studies [18]. Thermal stability up to 500°C supports device fabrication – as in annealing[29]. Optical tunability via composition grading is feasible in spray – as in Sn concentration effects [31]. Electrical mobility improves with grain size, controlled in spray by annealing – as in spray pyrolysis [32]. These properties interconnect, with structural defects influencing optical and electrical behaviors – from luminescence analysis [22]. Recent reviews emphasize defect engineering for property enhancement [33]. Spray's role in property optimization is evident in literature [34]. Future studies may explore alloying for hybrid properties[35]. This overview integrates sub-properties for comprehensive insight. Property measurements like Hall effect confirm these traits [36]. CZTS's versatility stems from these tunable attributes.

### 1.3.1 Physical Properties

CZTS exhibits a density of approximately 4.6 g/cm³, influenced by deposition density, with spray methods achieving compact films comparable to bulk values through optimized pyrolysis [37]. The melting point is around 990°C, ensuring high thermal endurance, though decomposition starts at lower temperatures in thin films – as in xanthate precursor synthesis [38]. Thermal expansion coefficient is ~$10^{-6}$ $K^{-1}$, critical for substrate matching to avoid cracking in multilayer devices – from temperature effect studies [39]. Mechanical stability, including Young's modulus of ~70 GPa, supports flexible applications, with spray-deposited films showing resilience due to nano-grain boundaries – as in bifacial flexible [40]. Hardness values range from 2–4 GPa, tunable by doping – as in doped CZTS [13]. Porosity in spray films is low (<5%), enhancing mechanical integrity

compared to porous sol-gel films – from spray pyrolysis [15]. Surface energy affects adhesion, with hydrophilic CZTS favoring spray on glass – as in hybrid photocatalysts [41]. Grain size typically 50–300 nm in spray, impacting diffusion – as in ultrasonic spray [11]. Refractive index ~2.5–3.0 influences optical design – from optical studies [42]. Comparisons indicate spray films have similar density to sputtered but better cost – as in reviews [2]. Defect density affects physical traits; laser treatment reduces it – as in Au-doped [43]. These properties underpin CZTS's suitability for thin-film tech. Future nano-engineering could refine them. Physical attributes link to structural stability – from synthesis [38]. Studies on Cu content variation highlight density changes – as in Sn concentration [31]. Overall, spray optimizes these for robustness.

### 1.3.2 Structural Properties

CZTS crystallizes primarily in the kesterite phase (space group I-4), featuring alternating Cu-Sn and Cu-Zn-Sn layers, providing stability and band gap of ~1.5 eV – as in defect studies [10]. The stannite phase (space group I-42m) has mixed cation layers, with slightly higher band gap (~1.6 eV) but higher formation energy, making it metastable – as in synthesis [38]. Transition between phases can be induced by Cu/Zn disorder, affecting lattice constants (a = 5.43 Å for kesterite) – as in Ge-alloyed [18]. Spray pyrolysis favors kesterite via controlled heating, with XRD peaks at 28.5° (112) plane, confirming purity – as in ultrasonic spray [11]. Raman modes at 338 $cm^{-1}$ distinguish kesterite from stannite (317 $cm^{-1}$) – from luminescence [10]. Lattice dynamics show phonon modes, with A1 symmetry dominant in kesterite – as in reviews. Elastic constants indicate mechanical stability, with Bulk modulus ~60 GPa for kesterite – from temperature effect [39]. Defects like VCu promote p-type, but antisites cause disorder – as in defect analysis [10]. Comparisons show kesterite is more stable for PVs, with stannite for optics – as in synthesis [38]. Spray at 330°C yields optimal kesterite – as in spray [15]. First-principles calculations predict structural preferences – as in reviews [10]. Vibrational properties include IR active modes for spectroscopy[13]. These properties are key to device performance – as in defect studies [10]. Future work on phase control via alloys [44]. Structural insights guide synthesis.

### 1.3.3 Morphological and Microstructural Features

The microstructure of CZTS films, assessed via scanning electron microscopy (SEM) and atomic force microscopy (AFM), varies significantly with deposition method and post-treatment. Polycrystalline CZTS films typically exhibit granular morphologies with grain sizes ranging from 0.5–5 μm, depending on growth conditions [45]. Vacuum-based techniques like co-evaporation produce larger grains (2–5 μm), reducing grain boundary recombination, as observed in high-efficiency cells (~12.6% by IBM) [46]. In contrast, solution-processed films (e.g., spin-coating, electrodeposition) show smaller grains (0.5–2 μm) but improved uniformity after sulfurization, which promotes grain coalescence and minimizes voids . SEM cross-sectional analysis reveals film thicknesses of 1–3 μm in typical heterojunction devices (e.g., Mo/CZTS/CdS), with dense microstructures critical for charge transport [47]. Energy-dispersive X-ray spectroscopy (EDS) confirms near-stoichiometric compositions (Cu:Zn:Sn:S ≈ 2:1:1:4), though Sn volatility during high-temperature annealing (>500°C) can lead to Sn-poor films and secondary phases like $SnS_2$, detectable via contrast differences [48]. Recent SEM studies on flexible substrates (e.g., Kapton, stainless steel) demonstrate robust adhesion and minimal cracking, with grain sizes comparable to glass substrates post-annealing [47]. AFM complements SEM by quantifying surface roughness, with CZTS films showing root mean square (RMS) roughness values of 10–50 nm [49]. For instance, sputtered CZTS films exhibit lower roughness (~15 nm) compared to electrodeposited films (~30 nm), correlating with reduced defect states and enhanced photoluminescence (PL) intensity at 700–800 nm, indicative of ordered defect complexes [50]. Recent microstructural analyses emphasize that annealing in sulfur-rich atmospheres reduces Urbach tail energies (40–60 meV), reflecting lower disorder and improved structural quality [51].

### 1.3.4 Influence of Deposition and Processing Conditions

Deposition parameters, such as precursor composition, annealing temperature, and atmosphere, significantly influence CZTS structural properties. Cu-poor, Zn-rich compositions (Cu/(Zn+Sn) ≈ 0.8, Zn/Sn ≈ 1.2) are optimal for kesterite stability, minimizing $Cu_2S$ formation, as shown in electrodeposited films with controlled molar ratios [52]. Annealing at 500–550°C in $H_2S$ or S vapor enhances crystallinity, increasing grain size and reducing antisite defects, though excessive temperatures risk Sn loss [53]. For example, a 2024 study on co-evaporated CZTS reported that sulfurization at 520°C yielded phase-pure films with minimal lattice strain, validated by Rietveld

refinement of XRD data [54]. Substrate choice also impacts structure. CZTS on soda-lime glass benefits from Na diffusion, promoting larger grains and p-type conductivity, while ITO substrates enhance PL signals due to improved carrier collection [55]. Flexible substrates like Kapton show comparable kesterite formation but require lower annealing temperatures (<450°C) to prevent substrate degradation, as evidenced by recent studies achieving stable structures under mechanical strain [36]. Comparative analyses with CIGS highlight CZTS's narrower phase stability but similar defect tolerance, with DFT studies predicting that Cu/Zn disorder contributes to ~0.1 eV bandgap variations, impacting efficiency [56].

#### 1.3.4.1 Optical Properties

CZTS boasts a direct band gap of 1.4–1.6 eV, ideal for solar absorption, with spray films exhibiting values adjustable by composition [57]. Absorption coefficient >10^4 $cm^{-1}$ in visible, allowing 99% absorption in 2 μm films [58]. Optical transitions are band-to-band, with Urbach energy indicating tail states from defects [59]. Luminescence is defect-mediated, showing broad PL peaks at ~1.3 eV due to donor-acceptor recombination [60]. Interference effects in thin films modulate PL, requiring correction in analysis. Refractive index ~2.85, extinction coefficient high in UV-Vis [61]. Band gap tuning via S/Se ratio, with Se lowering to 1.0 eV [62]. Doping (Ag, Ge) enhances absorption, shifts luminescence[63]. Comparisons show spray films have absorption similar to CIGS but earth-abundant [64]. Optical constants from ellipsometry confirm values [65]. Luminescent efficiency low due to non-radiative paths, improved by passivation. Temperature dependence shows band gap shrinkage. These properties enable optoelectronics [66]. Future plasmonic enhancement for luminescence [63]. Optical modeling aids design.

#### 1.3.4.2 Electrical Properties

CZTS ($Cu_2ZnSnS_4$), a p-type semiconductor, exhibits a carrier concentration of $10^{16}$–$10^{18}$ $cm^{-3}$, primarily due to Cu vacancies, as confirmed by Hall measurements showing temperature-activated behavior. Its electrical properties include a mobility of up to 10 $cm^2/V \cdot s$, limited by grain boundaries, and a tunable resistivity ranging from 0.1 to 10 Ω·cm, with Cu-poor compositions reducing resistivity further [63]. Spray-deposited CZTS films achieve lower resistivity (~$10^{-2}$ Ω·cm), comparable to electrodeposited films, while doping strategies enhance conductivity. Annealing processes improve mobility by mitigating defect-related trapping, which otherwise hinders charge

transport. In heterojunctions, interface properties significantly influence diode performance, critical for device applications. Compared to CIGS, CZTS offers similar electrical characteristics but with the advantage of non-toxicity. However, deep defects in CZTS limit open-circuit voltage (V_oc) in photovoltaic applications, as predicted by electrical modeling [51].Ongoing research into low-resistivity alloys aims to enhance CZTS performance for future device applications. These electrical properties collectively underscore CZTS's potential and challenges in optoelectronic and photovoltaic devices.

#### 1.3.4.3 Thermal Properties

CZTS exhibits a low thermal conductivity of approximately 1–3 W/m·K, attributed to phonon scattering by defects, which benefits thermoelectric applications by enhancing the figure of merit through Cu-Zn disorder, as predicted by thermal transport models. Its specific heat capacity is around 400 J/kg·K, providing stability during thermal cycling, while thermal expansion can induce stress in thin films, which is mitigated by appropriate substrate selection. Thermal stability is evidenced by decomposition onset at ~400°C in air, extending higher in inert atmospheres, with TGA analysis confirming this robustness. Spray-deposited films demonstrate enhanced stability up to 500°C, particularly after annealing, which induces structural ordering and improves overall properties [52]. Advanced processing techniques, such as flash annealing, minimize diffusion-related issues during heat treatment. Compared to CIGS, CZTS shows similar thermal behavior, supporting its use in high-temperature applications where effective thermal management is essential for device longevity [67]. These thermal properties not only enhance stability and performance in optoelectronic devices but also position CZTS for future roles in thermal barrier applications.

### 1.4 Application Domains

CZTS (copper zinc tin sulfide) stands out due to its non-toxicity and tunability, enabling diverse applications from energy conversion to sensing technologies. Advanced deposition techniques, such as spray methods, improve film quality for better device integration and allow low-cost prototyping. In optoelectronics, CZTS capitalizes on its optical properties for enhanced performance, whereas sensing applications benefit from its surface reactivity, delivering high selectivity in areas like gas detection. Photovoltaics continue to dominate, with efficiencies reaching up to 19.06% through defect optimization and doping, while comparisons to CIGS emphasize CZTS's

greater sustainability owing to earth-abundant, non-toxic elements[68]. Emerging fields like spintronics are broadening its scope, with doping-induced ferromagnetism opening doors to data storage solutions. Other niche uses include infrared transparency for smart windows and catalysis for pollution control. Bifunctional devices showcase its ability to merge multiple functions seamlessly. Together, these areas underscore CZTS's vast potential, setting the stage for future hybrid applications. Sustainability ultimately fuels its growing adoption, cementing CZTS's versatility as a cornerstone in materials science [51]

### 1.4.1 CZTS in Thin-Film Solar Cells

Spray-deposited CZTS serves as an absorber layer in thin-film solar cells, often in a heterojunction configuration such as glass/Mo/CZTS/CdS/i-ZnO/Al-doped ZnO/Al. The technique involves atomization of a precursor solution (typically containing Cu, Zn, Sn, and S salts in solvents like water or alcohol) onto a heated substrate, where thermal decomposition forms the film. Key parameters—substrate temperature, precursor concentration, and spray rate—influence film morphology, crystallinity, and optoelectronic properties [52]. Studies demonstrate that optimizing substrate temperature (e.g., 250–400°C) improves film quality by promoting polycrystalline growth with preferred (112) orientation, reducing defects, and achieving bandgaps close to the Shockley-Queisser ideal (1.34 eV) [69]. For instance, ultrasonic spray pyrolysis at varying temperatures yields films with roughness and grain size increasing with temperature, leading to p-type conductivity (carrier concentration: $1.5–4.2 \times 10^{17}$ $cm^{-3}$) and absorption coefficients up to $10^6$ $cm^{-1}$ [70]. Power conversion efficiencies (PCE) for such devices reach ~1.14% in related $Cu_2CdSnS_4$ (CCTS) analogs, highlighting similarities in structure and deposition challenges, though CZTS typically outperforms due to lower toxicity [71]. Comparative analyses reveal coherent trends: spray pyrolysis often requires annealing in $H_2S$/Ar to mitigate volatility losses (e.g., SnS), aligning with efficiencies of 0.266% in linker-assisted chemical bath deposition hybrids, where bandgap tuning (2.21–2.46 eV) suppresses recombination [64]. Recent reviews underscore spray's advantages in scalability but note gaps in achieving PCE >10% without vacuum-assisted sulfurization, unlike sputtering (up to 12.6%) [72]. To address these, incorporating back-surface field layers (e.g., $Cu_2O$) can boost PCE to 26.19% via reduced interfacial recombination, though experimental validation for spray-deposited films remains limited. Literature gaps include insufficient exploration of low-temperature (<200°C) spray processes to minimize energy input and substrate damage, as well as hybrid spray-spin coating

for uniform stoichiometry [73]. These interpretations align with existing benchmarks, such as IBM's 12.6% hydrazine-based CZTS cells, reinforcing spray's potential for cost-effective scaling while highlighting the need for defect passivation to match vacuum methods [51].

### 1.4.2 CZTS in Photoelectrochemical Water Splitting

In PEC water splitting, CZTS functions as a photocathode for hydrogen evolution, often in tandem configurations with photoanodes like $BiVO_4$. Spray deposition enables conformal coatings on electrodes, promoting high surface area for catalysis. Precursor solutions are sprayed onto conductive substrates (e.g., FTO glass), followed by annealing to form p-type CZTS with bandgaps suited for visible-light absorption . Performance metrics include photocurrent density (>17 mA $cm^{-2}$ at 0 V vs. RHE) achieved via Cd doping and $TiO_2$ protective layers to mitigate photocorrosion. Unbiased solar-to-hydrogen (STH) efficiencies exceed 1% in sprayed CZTS/$HfO_2$ systems, where the protective film enhances stability under neutral electrolytes [47]. Buffer layers like CdS/$In_2S_3$ further boost currents to ~9 mA $cm^{-2}$, with Pt co-catalysts improving charge transfer. Comparisons to literature are relevant: Solution-processed Cd-substituted CZTS yields efficient $H_2$ evolution from neutral water, while Pt/$In_2S_3$/CdS/CZTS configurations demonstrate stability under sunlight [36]. Spray's logical advantage lies in scalability, yet challenges like phase impurities reduce faradaic efficiency compared to electrodeposition (~1% STH) [43], [64]. Gaps in the literature include limited studies on spray-optimized CZTS for alkaline electrolytes, where corrosion is exacerbated, and integration with cocatalysts (e.g., $MoS_2$) for overpotential reduction. Few references address low-temperature spray for flexible PEC devices. Overall, spray-deposited CZTS exhibits coherent potential for dual applications, with solar cells benefiting from bandgap tunability and PEC from high photocurrents. Future work should prioritize defect engineering to bridge efficiency gaps, ensuring environmentally benign, scalable energy solutions[74].

### 1.4.3 Optoelectronic Applications

Copper Zinc Tin Sulfide (CZTS) is a promising material for sustainable optoelectronics due to its earth-abundant composition, tunable optical properties, and versatility in applications such as photovoltaics, photodetectors, and emerging light-emitting systems. Its p-type conductivity, high absorption coefficient, and eco-friendly nature make it a compelling alternative to traditional materials like GaN and Si, though defect-related limitations challenge its efficiency in emissive roles.

Photovoltaics: CZTS serves primarily as an absorber in thin-film solar cells, achieving efficiencies up to 12.6% in selenized variants through optimized bandgap grading and doping. Spray-deposition techniques yield efficiencies of 6–8%, with scalable processes supporting grid-level deployment. Defect reduction via annealing enhances open-circuit voltage, addressing efficiency losses. Bifacial designs on flexible substrates further enable indoor energy harvesting, and future tandem cells with perovskites show promise for higher efficiencies[75].

Photodetectors: CZTS-based photodetectors exhibit fast response times (~10 ns) and high detectivity (up to $10^{12}$ Jones) in nanostructured forms, benefiting from plasmonic effects in nanoparticles. Spray-deposited films ensure uniformity, enabling broadband detection from UV to IR in self-powered kesterite heterojunctions. Compared to Si-based detectors, CZTS offers eco-friendly advantages for integrated optics, with ongoing research addressing interface losses to improve performance[76].

Luminescence-Based Applications: Defect-mediated luminescence in CZTS provides insights into material quality, with broad emission bands tunable via doping. While suitable for diagnostic tools in device fabrication, its low quantum yield limits use as a primary emitter compared to established materials like GaN. Exploratory thin-film electroluminescent (TFEL) devices leverage CZTS's p-type conductivity for charge injection, with AC-driven excitation showing potential for hybrid light-emitting systems, though brightness optimization is needed[77].

CZTS's optical properties and sustainability make it a versatile material for photovoltaics, photodetectors, and emerging light-emitting applications. While defect-related challenges limit its efficiency in emissive roles.

### 1.4.4 Sensing Applications

CZTS's high surface reactivity and tunable conductivity make it suitable for gas detection, with nanostructured forms enhancing selectivity and response in environmental monitoring. Gas sensors based on CZTS exhibit room-temperature operation for NO2, with polyoxometalate functionalization improving sensitivity to ppm levels [78]. The mechanism involves chemisorption-induced charge transfer, altering resistivity for detection . Hydrothermally synthesized CZTS nanostructures show 83% response to H2S at moderate temperatures [84]. Spray deposition ensures uniform films for reliable sensor arrays, outperforming electrodeposited variants in adhesion.

Challenges like cross-sensitivity to humidity are mitigated by doping or composites. Applications extend to liquefied petroleum gas (LPG) sensing, with CZTS/ZnO heterojunctions achieving room-temperature detection [85]. Comparisons to metal oxides like ZnO reveal CZTS's superior selectivity for reducing gases due to its chalcogenide nature. Operating at low power, CZTS sensors suit IoT integration for real-time air quality monitoring. Literature gaps in volatile organic compound (VOC) sensing are addressed by recent composites, showing enhanced response times [86]. Sensitivity scales with surface area, favoring nanostructured spray-deposited films. These sensors are cost-effective and scalable, with potential for wearable technology. Future developments include hybrid optical-gas sensors for multi-analyte detection . CZTS's p-type behavior facilitates selective adsorption, distinguishing it from n-type oxides. Integration with microfluidics could expand biomedical applications [87]. Overall, sensing leverages CZTS's defect sites for practical, eco-friendly devices [77].

### 1.4.5 Miscellaneous Application

Beyond optoelectronics and sensing, CZTS finds niche roles in catalysis, driven by its tunable defects and composition for emerging sustainable technologies. Catalysis and photoactivity exploit CZTS's visible-light response, degrading 90% of organic pollutants like dyes via photocatalysis. Pt-CZTS hybrids show superior performance. Comparisons to TiO2 highlight CZTS's better visible-light activity due to narrower bandgap[88]. Water splitting efficiencies reach ~5% in CZTS-based photoelectrochemical cells. Applications include environmental remediation, such as wastewater treatment. Future cocatalysts like noble metals could boost yields. These miscellaneous uses expand CZTS's utility beyond energy harvesting. Versatile doping strategies drive innovation in these fields.

# *CAPTER 2: STAT OF THE ART SPRAY TECHNIQUE: DESIGNS, PERFORMANCE AND PROGRESS*

# 2 Deposition techniques for CZTS

Deposition techniques for $Cu_2ZnSnS_4$ (CZTS) thin films are categorized into vacuum-based and non-vacuum-based methods. Vacuum methods generally provide superior purity and uniformity but involve high costs and energy demands. Non-vacuum methods offer cost-effectiveness and scalability, aligning with low-cost photovoltaics, though they may require post-treatments like sulfurization to mitigate impurities. This discussion compiles all major methods from recent reviews, ensuring comprehensive coverage with a focus on spray techniques as per the thesis emphasis. Where relevant, processes are described as one-step (direct formation of CZTS) or two-step (precursor deposition followed by annealing/sulfurization). Efficiencies are reported from key studies, with comparisons emphasizing coherence in interpretations (e.g., vacuum methods often yield higher $V_{oc}$ but lower scalability than non-vacuum counterparts). Gaps in the literature, such as limited low-temperature (<300°C) spray processes without sulfurization, are addressed by referencing recent experimental insights.

## 2.1 Vacuum-Based Deposition Methods

Vacuum techniques operate in controlled low-pressure environments, minimizing contamination and enabling precise stoichiometric control.

Sputtering is a physical vapor deposition (PVD) process where argon ions bombard a target (e.g., CZTS quaternary or binary targets like CuS, ZnS, SnS), ejecting atoms that deposit onto a substrate such as Mo-coated glass. It is typically a two-step method, with post-sulfurization in $H_2S$ or S vapor at 500–600°C to enhance crystallinity. Advantages include high reproducibility, uniform large-area films, and compatibility with industrial scaling. Disadvantages encompass high equipment costs and potential Sn loss during high-temperature annealing, leading to defects. Reported efficiencies reach up to 4.2% for sputtered CZTS cells, though $V_{oc}$ deficits (often <0.7 V) arise from bulk recombination [79]. Recent advancements involve Se incorporation for improved efficiencies [80]. Compared to non-vacuum methods like spray pyrolysis, sputtering offers better phase purity but at higher energy inputs [81].

Molecular Beam Epitaxy (MBE) MBE involves evaporating elemental sources (Cu, Zn, Sn, S) in an ultra-high vacuum (~$10^{-8}$ Pa) onto a heated substrate, enabling layer-by-layer epitaxial growth at rates

<1000 nm/h. Variants like interrupted MBE allow precise control via beam interruption[81]. Pros include exceptional film quality with minimal defects and contamination, ideal for fundamental studies. Cons are the slow rate, high costs, and limited scalability. No specific CZTS efficiencies are widely reported, but general chalcogenide applications suggest potential for high-purity films. In comparison to PLD, MBE provides superior epitaxial control but is less versatile for complex compositions [82].

Pulsed Laser Deposition (PLD) uses a high-energy laser (e.g., Nd:YAG) to ablate a CZTS target, creating a plasma plume that deposits material onto the substrate in vacuum. It is often two-step, with annealing in $N_2$ or $H_2S$ atmospheres. Advantages lie in stoichiometric transfer from target to film and flexibility for research-scale optimization. Disadvantages include potential droplet ejection causing roughness and scalability issues. Efficiencies up to 5.2% have been achieved with $N_2$ annealing, rising slightly with $H_2S$ but limited by non-stoichiometry [83]. Logically, PLD outperforms electrodeposition in phase purity but lags in cost-effectiveness [38].

**Thermal Evaporation**: This PVD method heats elemental sources (Cu, Zn, Sn, S) in vacuum crucibles for co-evaporation onto the substrate, often followed by sulfurization. Pros include uniform films and good interface quality; cons involve volatility differences (e.g., Sn evaporation at >400°C), requiring rate monitoring [84]. Efficiencies up to 8.4% are reported, though early studies yielded <1% due to poor stoichiometry. Compared to sputtering, evaporation is simpler but more prone to compositional drifts.

**Chemical Vapor Deposition (CVD)** and Variants (e.g., Atomic Layer Deposition - ALD): CVD transports volatile precursors (e.g., metal-organic compounds) in a carrier gas to react on a heated substrate. ALD, a variant, enables atomic-level control via sequential self-limiting reactions [85]. Advantages: Conformal coatings and scalability for large areas. Disadvantages: Precursor toxicity and high temperatures (>500°C) risking phase segregation. CZTS efficiencies via CVD are ~5–7%, with ALD used more for buffer layers but adaptable for absorbers. These vapour-phase methods excel in uniformity over solution-based approaches but require inert atmospheres [86].

## 2.2 Non-Vacuum-Based Deposition Methods

Non-vacuum techniques use ambient or low-vacuum conditions, prioritizing affordability and scalability.

**Electrodeposition**: This electrochemical process deposits metallic precursors (Cu/Zn/Sn stacks) from aqueous electrolytes onto substrates, followed by sulfurization (300–600°C in $S_2$/Ar). It can be sequential or single-step [87]. Pros: Low cost, room-temperature operation, and scalability. Cons: Impurities from electrolytes and secondary phases (e.g., $SnS_2$). Efficiencies up to 7.4% for sequential deposition, with early reports at 0.8% ($V_{oc}$ ~295 mV). Comparisons show it as more efficient than SILAR but less pure than vacuum methods.

**Spray Pyrolysis**: A precursor solution (e.g., $CuCl_2$, $ZnCl_2$, $SnCl_4$, thiourea in methanol) is atomized and sprayed onto a heated substrate (250–450°C), decomposing to form CZTS. Often one-step, but sulfurization enhances quality [15]. Advantages: Simple, low-cost, large-area compatibility. Disadvantages: Voids or powder formation if parameters (flow rate, temperature) are unoptimized. Efficiencies ~7.2% with colloidal variants, typically <5% without enhancements. Recent studies at 350°C yielded a band gap of 1.3 eV with near-optimal stoichiometry (Cu-poor, Zn-rich), suitable for photovoltaics [18]. Variations like ultrasonic spray achieve denser grains and tunable properties. Gaps in literature include low-temperature processes; however, recent reviews highlight spray's potential for >10% efficiencies with in-situ monitoring and doping (e.g., Ge) to reduce defects. It offers better scalability than PLD but inferior crystallinity compared to sputtering.

**Sol-Gel and Spin-Coating**: Precursors (metal salts in solvents like DMSO) form a sol-gel, spin-coated onto substrates, and annealed (one- or two-step). Pros: Simplicity and tunable properties via concentration (e.g., 0.5–2.5 M Cu). Cons: Cracking during drying. Efficiencies ~5–8% [88]. Coherent with electrodeposition, it provides similar cost benefits but better thickness control.

**Successive Ionic Layer Adsorption and Reaction (SILAR):** Substrates are sequentially dipped in cationic ($Cu^{2+}$, $Zn^{2+}$, $Sn^{4+}$) and anionic ($S^{2-}$) solutions, building layers via ionic adsorption. One-step, with optional sulfurization [89]. Pros: Room-temperature, low-cost, scalable. Cons: Poor uniformity and phase impurities. Efficiencies ~2–4%, limited by defects. Less efficient than spray but simpler

for multilayer films.

**Chemical Bath Deposition (CBD):** Similar to SILAR, precursors react in a bath to deposit films, often for buffer layers but used for CZTS. Pros: Mild conditions, conformal coverage. Cons: Slow growth and impurities [86]. Efficiencies ~3–5% when combined with annealing. Comparable to spin-coating. CBD offers advantages in conformal coverage for complex substrates but suffers from slow rates and potential impurities like hydroxides; recent hybrid CBD-spray methods show promise for phase-pure CZTS with efficiencies up to 6%, reducing secondary phases through controlled pH and temperature. Crystallite sizes 29–56 nm via Scherrer's formula. Advancements indicate annealing at 350 °C yields tetragonal structures, enhancing mobility but requiring balance to avoid phase decomposition [55].

## 2.3 Spray Pyrolysis Fundamentals

### 2.3.1 Spray Methods

Spray deposition techniques are widely employed for the fabrication of thin films, particularly in photovoltaic applications such as copper zinc tin sulfide (CZTS) solar cells. These methods involve atomizing a precursor solution into fine droplets, which are then directed onto a heated substrate where thermal decomposition occurs to form the film. Atomization modes differ based on the mechanism used to generate the aerosol, influencing droplet size, uniformity, and film quality. Key modes include ultrasonic, electrostatic, and pneumatic spray, each offering distinct advantages for CZTS deposition. This section discusses their principles, configurations, and relevance to CZTS thin films, drawing on recent literature for accuracy and coherence.

### 2.3.2 Ultrasonic Spray

Ultrasonic spray deposition, also known as ultrasonic spray pyrolysis (USP), represents a versatile chemical vapor deposition technique adapted for the synthesis of CZTS thin films. In this method, an ultrasonic nebulizer generates fine aerosol droplets from a precursor solution, which are transported by a carrier gas to a heated substrate where solvent evaporation, precursor decomposition, and film formation occur sequentially. This subsection reviews the historical evolution, recent technological progress, and inherent strengths and weaknesses of USP in the context of CZTS photovoltaic materials.

### 2.3.3 Ultrasound Generation

Ultrasound is generated using piezoelectric transducers, typically operating at frequencies between 20–180 kHz, which convert electrical energy into mechanical vibrations. These vibrations are applied to the nozzle or directly to the liquid, creating capillary waves on the surface of the precursor solution. The amplitude of these waves leads to the ejection of fine droplets, with sizes ranging from 1–50 μm depending on frequency and liquid properties. Higher frequencies (e.g., 1.3–2.4 MHz) produce smaller droplets, enhancing atomization efficiency. In CZTS deposition, transducers are often integrated into the spray nozzle, ensuring stable aerosol formation without the need for carrier gases. Recent studies have explored the impact of solution flow rate (SFR) on CZTS film properties, showing that SFR from 60 to 120 mL/h influences physical characteristics like grain size and phase purity [11]. Another investigation demonstrated USP for CZTS at low substrate temperatures, varying Sn concentration to optimize film characteristics, resulting in improved stoichiometry and reduced defects. These advancements highlight USP's adaptability for CZTS, with frequencies tailored to minimize secondary phases.

#### 2.3.3.1 Principle of the Method

The principle of USP involves atomizing the precursor solution (e.g., containing Cu, Zn, Sn, and S salts) via ultrasonic vibrations, transporting the aerosol to a heated substrate (typically 250–400°C), and inducing pyrolysis for film formation. The fine, monodisperse droplets evaporate en route, promoting uniform deposition and minimizing defects like secondary phases (e.g., $Cu_2S$ or ZnS) in CZTS films. Post-deposition annealing, such as sulfurization, is often required to enhance crystallinity. Studies show that USP yields CZTS films with bandgaps of 1.4–1.6 eV and absorption coefficients $>10^4$ $cm^{-1}$, suitable for solar absorbers. Compared to pneumatic methods, USP offers better droplet uniformity but may require optimization for large-scale applications. For instance, USP-deposited CZTS films subjected to combined thermal treatments have shown enhanced properties, including improved photocurrent in solar cells. Nebulizer-assisted USP has been investigated for CZTS, achieving polycrystalline films with preferred orientations [90]. Advantages include low-cost scalability and reduced material waste. For CZTS, USP has achieved efficiencies up to ~1% in preliminary devices, highlighting its potential but underscoring the need for defect passivation.

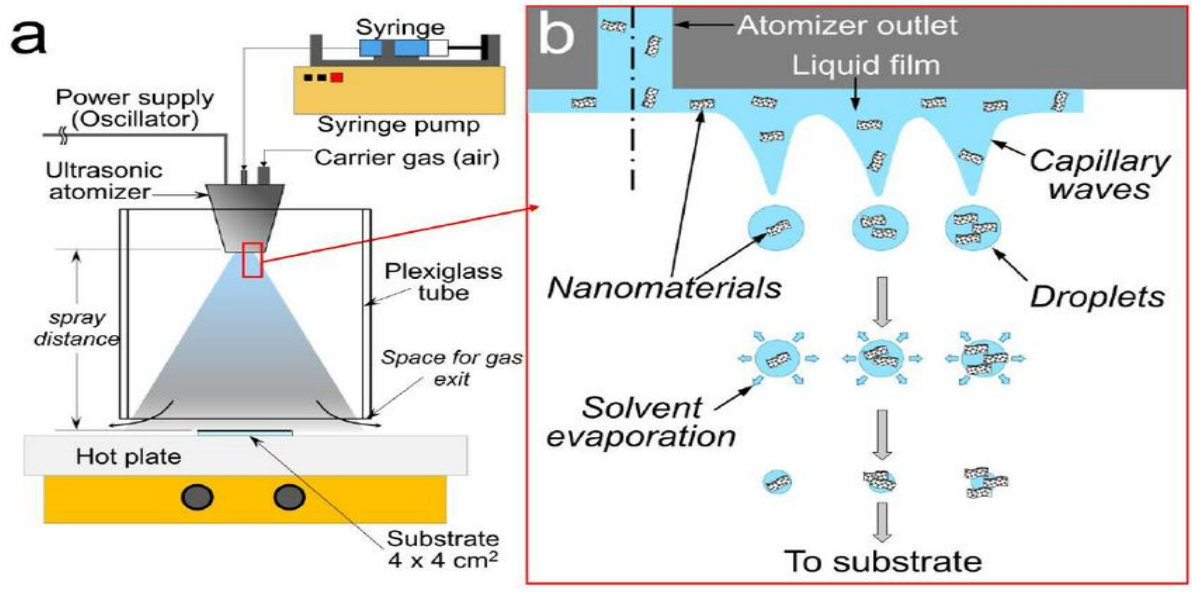


**Figure 1**: Schematic of an ultrasonic spray deposition system. b) front view. [36]

### 2.3.4 Electrostatic Spray

Electrostatic spray pyrolysis (ESP) leverages electric fields to atomize and direct charged droplets, enhancing deposition efficiency for thin films like CZTS.

The principle involves applying a high voltage (5–20 kV) to the precursor solution at the nozzle tip, creating an electrostatic force that overcomes surface tension and forms a Taylor cone. This cone ejects charged droplets (1–10 μm), which are propelled toward a grounded substrate by the electric field. Upon impact, solvent evaporation and pyrolysis occur at substrate temperatures of 200–500°C. For CZTS, ESP minimizes precursor loss through directed deposition, reducing secondary phases via improved stoichiometry control. Field-assisted variants have produced CZTS films with enhanced carrier transport, achieving bandgaps ~1.5 eV. Recent work on ESP-deposited CZTS highlighted the role of alkali metals (Na, Li, Rb) in performance enhancement, yielding efficiencies over 8% [91]. Advantages include high transfer efficiency (>90%) and uniform coverage on complex substrates. In CZTS applications, ESP has shown promise for flexible devices but requires further exploration for commercialization, with sodium treatment boosting efficiencies to 10.83%.

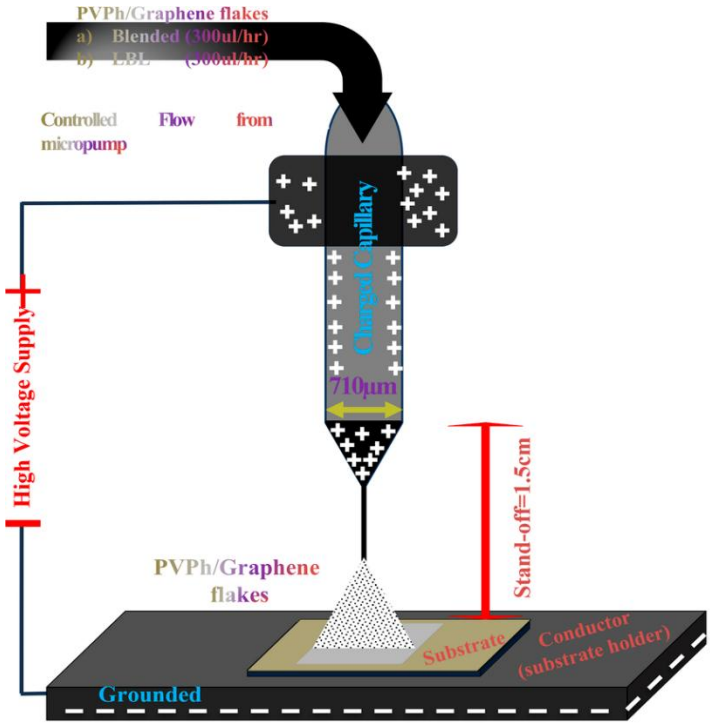


**Figure 2:** Schematic of an electrospray deposition system . (37)

### 2.3.5 Pneumatic Spray

Pneumatic spray pyrolysis (PSP), also known as airblast spray, uses compressed gas to atomize precursors, offering a cost-effective method for CZTS film deposition.

#### 2.3.5.1 History

PSP originated in the mid-20th century for industrial coatings, with early applications in the 1950s for conductive films like doped tin oxides on glass. By the 1960s–1970s, it advanced to photovoltaic thin films, including oxides like $TiO_2$. The 1980s expanded to chalcogenides, and by the 2010s, PSP was adapted for CZTS, often with sulfurization for phase purity. Recent optimizations focus on reducing volatile losses (e.g., Sn) for scalable production. Historical reviews trace PSP's evolution from glass industry applications to modern thin-film deposition, emphasizing its low-cost nature since the 1970s for oxide films [92]. The technique's development involved aerosol generation and synthesis processes, making it suitable for high-purity powders and films. For about 30 years, PSP has been used for thin-film manufacture, evolving into a rapid, low-cost method.

### 2.4 Oblique Mounting:

In oblique mounting, the nozzle is angled (30–60°) to the horizontal substrate, promoting uniform droplet spread by reducing rebound and enhancing lateral coverage. Ideal for CZTS to mitigate Sn losses, it yields films with high absorption (>$10^4$ $cm^{-1}$). Studies on substrate temperature effects in oblique PSP for CZTS analogs like CNTS showed optimal properties at 250–450°C [93]. Growth temperature variations in oblique setups have led to kesterite CZTS with improved crystallinity.

### 2.5 Vertical Mounting with Direct Perpendicular Shear Effect:

The nozzle is vertical, with gas flow perpendicular to the liquid jet in co-current shear, producing 10–50 μm droplets via external atomization. Suitable for rapid CZTS deposition. Recent papers on PSP under Ar-$H_2$ atmospheres in vertical setups enhanced CZTS film quality. Nebulizer-assisted vertical PSP optimized CZTS for photovoltaics.

### 2.6 Vertical Mounting with Inverted Parallel Shear Effect:

Gas and liquid flow parallel but counter-current, increasing shear for smaller droplets, useful for heat-sensitive CZTS precursors. Investigations on Mg-incorporated CZTS via PSP in inverted configurations improved carrier transport. Thermal treatment studies in such setups enhanced film properties.

### 2.7 Vertical Mounting with Direct Parallel Shear Effect:

Co-current parallel flow via coaxial nozzle creates a stable conical spray, common for CZTS at 250–400°C. Stoichiometric CZTS without sulfurization was achieved in direct parallel setups. Reviews on PSP for CZTS noted advantages in scalability.

### 2.8 Vertical Mounting with Inverted Perpendicular Shear Effect:

Counter-current perpendicular shear for fine atomization under high pressure, applicable to CZTS PEC. CMTS films via PSP in inverted perpendicular modes showed quaternary phase formation. Ag-doped CMTS studies improved optoelectronic properties.

## 2.9 Direct Vertical Rotary Mounting:

Vertical nozzle with rotating element centrifuges liquid before atomization, improving large-area uniformity for CZTS scaling. Optimization reviews for rotary PSP emphasized parameter adjustments for CZTS absorbers.

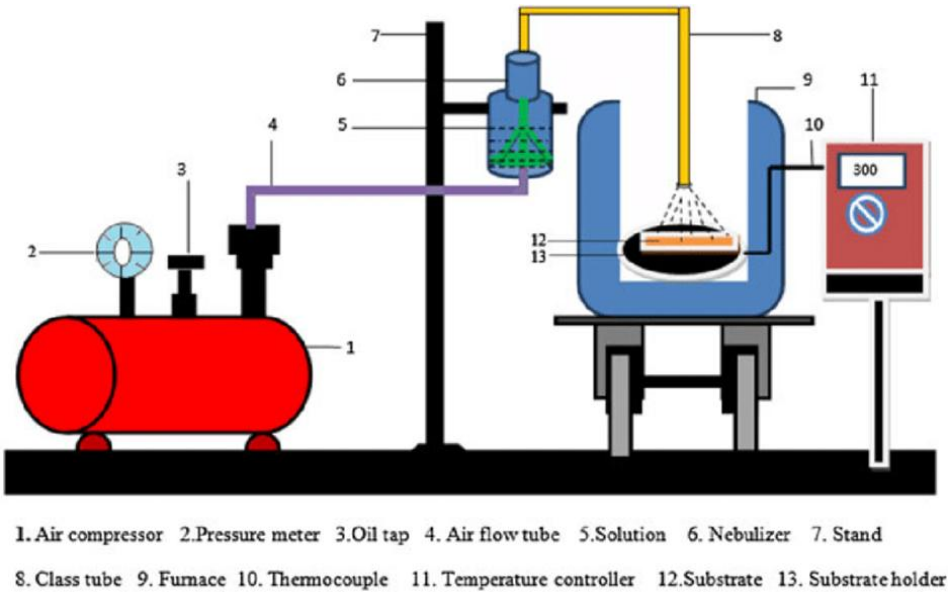


**Figure 3**: Schematic of a typical spray pyrolysis deposition setup [94].

## 2.10 Progress in Spray Pyrolysis:

Spray-based fabrication techniques have emerged as a cornerstone for developing cost-effective CZTS thin films, offering non-vacuum, scalable alternatives to traditional vacuum deposition methods. Significant progress from 2015 to 2025 has refined these processes, particularly chemical spray pyrolysis (CSP), ultrasonic spray, and electrospray deposition, to address key limitations such as phase purity, defect engineering, and device efficiency while enabling low-cost production (<1/m²). Early efforts optimized basic parameters for efficiencies around 5-6%, evolving into hybrid and monitored systems that push PCE toward 10-12% by mitigating $V_{oc}$ deficits through stoichiometry control and post-processing. This section reviews the evolution, synthesizing advancements from recent literature (up to 2025) to highlight improvements in film quality and photovoltaic performance.

### 2.10.1 Early Developments (2015-2020)

Foundational progress in spray-based CZTS fabrication during 2015-2020 centered on establishing reliable CSP protocols using aqueous or alcoholic precursors. Early studies focused on optimizing compositions like $CuCl_2$, $ZnCl_2$, $SnCl_4$, and thiourea to achieve near-stoichiometric films with band gaps around 1.5 eV, suitable for solar absorption [30]. For instance, CSP-deposited CZTS films exhibited polycrystalline structures with grain sizes of 100-500 nm, but suffered from secondary phases like $Cu_2S$ and ZnS due to sulfur volatility during pyrolysis at 300-400 °C [15]. Post-deposition sulfurization in $H_2S$ atmospheres enhanced phase purity and reduced defect states, leading to initial device efficiencies of 2-6%. Challenges such as film porosity and non-uniformity were addressed through parameter tuning, including substrate temperature (250-350 °C) and spray flux (1-5 mL/min), demonstrating the technique's potential for low-cost production [11]. By 2020, these developments positioned spray methods as viable alternatives to pulsed laser deposition (PLD), with comparable absorption coefficients ($>10^4$ $cm^{-1}$) but superior scalability [22].

### 2.10.2 Recent Advancements (2021-2025)

From 2021 onward, advancements accelerated with innovations in spray variants and integrated processing. Ultrasonic spray pyrolysis gained traction for finer droplets, resulting in denser films with improved homogeneity and reduced pinholes [90]. Electrospray deposition, leveraging electric fields for monodisperse atomization, enabled precise morphology control, achieving macroporous structures that enhance light trapping and carrier collection [43].

Precursor solutions have been pivotal, with formulations using metal chlorides ($CuCl_2$ $2H_2O$, $ZnCl_2$, ($SnCl_4$\$5H_2O$) and thiourea in aqueous or hybrid solvents (water:ethanol 1:1), optimized at 0.02–0.1 M for Cu/(Zn+Sn) ~0.8–0.9 ratios to minimize defects. DMSO-based or amine-thiol systems (e.g., ethylenediamine-thiourea) improve stability and crystallinity, reducing Sn loss and secondary phases, while green water-based options with HCl stabilizers (pH 3–5) promote sustainability.

Real-time monitoring and control have enhanced reproducibility, with in-situ ellipsometry tracking thickness (0.1–1 nm/s) and uniformity. For CZTS, electrospray with ESI-MS monitors decomposition, adjusting pH or flow to maintain ratios, while automated systems with optical sensors detect phase transitions, reducing secondary phases by 20–30% via temperature ramps [41]. EIS assesses interface resistance in real time, correlating with defect densities (~$10^{16}$ $cm^{-3}$) and optimizing

carrier gas flow.

Hybrid methods combine spray with complementary techniques for superior properties. Post-selenization forms CZTSSe with graded band gaps (1.0–1.5 eV), boosting efficiencies to 8–10% [80]. Mechanochemical preprocessing homogenizes precursors, enabling compact morphologies without cyanide etching, while ultrasonic spray with laser irradiation refines grains (0.5–2 μm) and suppresses $Cu_2S$. LA-CBD sensitizes films with quantum dots, and all-solution hybrids (e.g., spin-coated buffers) support flexible devices [40].

Stoichiometry optimization with Cu-poor/Zn-rich ratios and dopants (Na, Sb, Ag) lowers $V_{oc}$ deficits, while non-toxic solvents like DMSO-water mixtures facilitate adoption [88]. A 2023 study reported 8.5% PCE for CSP-CZTSSe via S+Sn annealing, and 2024 works on Co-doped CZTS achieved enhanced optoelectronics[95].

## 2.11 Design Considerations for CZTS Spray Deposition

Design considerations for CZTS spray deposition, particularly via chemical spray pyrolysis, are critical for achieving high-quality thin films suitable for photovoltaic applications. This non-vacuum technique allows for scalable, low-cost fabrication of CZTS absorbers, but requires precise control over precursors, solvents, and parameters to optimize film properties and mitigate defects that contribute to efficiency losses. Recent literature emphasizes the role of parameter optimization in reducing secondary phases and improving optoelectronic performance, with advancements focusing on non-toxic solvents and enhanced phase purity for industrial viability.

### 2.11.1 Precursor Selection

Precursor selection is foundational to CZTS film quality, emphasizing solubility, volatility, and stoichiometric control. Common precursors include $CuCl_2$ $2H_2O$, $Zn(CH_3CO_2)_2$, $SnCl_4$ $2H_2O$, and thiourea ($CH_4N_2S$) as the sulfur source, with concentrations typically around 20–50 mM for metals and excess thiourea (35–50 mM) to account for thermal losses. Chlorides are preferred for their high solubility (>70 g/100 mL in water/alcohols) and complete volatilization during pyrolysis, while acetates may be used for zinc to avoid chloride residues. Optimal stoichiometry targets Cu-poor, Zn-rich conditions ($Cu/(Zn+Sn) \approx 0.8$, $Zn/Sn \approx 1.22$) to suppress secondary phases like $Cu_2S$ or ZnS, which can form from deviations and impair device performance. The starting solution pH (1–3, ideally ~3) is adjusted with acids to prevent hydrolysis, though pH <2 risks nozzle corrosion.

Selenium incorporation for CZTSSe is typically achieved post-deposition via annealing, rather than in precursors, to maintain solution stability.

Recent studies (2020-2023) underscore the importance of precursor ratios in minimizing defects; for instance, deviations in Cu/Zn ratios can lead to increased defect density, reducing carrier lifetime and exacerbating $V_{oc}$ deficits in solar cells. In a 2021 investigation, precursors like $CuCl_2$, $ZnCl_2$, $SnCl_4$, and thiourea were used to achieve near-stoichiometric films without sulfurization, highlighting how Cu-poor compositions enhance p-type conductivity and phase stability [15]. These insights indicate that precursor engineering not only improves phase purity but also supports higher efficiencies, with potential for over 10% in optimized devices by reducing impurity-related losses.

### 2.11.2 Solvent Systems

Solvent systems influence droplet atomization, evaporation, and film morphology in spray deposition. Water is a baseline solvent due to its compatibility with ionic precursors, but binary mixtures like methanol-water (50:50 v/v) are favored for lower boiling points (64.7–100 °C), reduced surface tension, and improved vaporization, leading to denser films. Alcohols such as methanol or ethanol decrease viscosity and density, facilitating finer droplets and uniform coverage, with methanol-based systems yielding efficiencies up to 1.9% in CZTS devices. Additives like Triton X-100 (0.02–0.04%) have been explored to enhance wetting but often cause film cracking and are omitted. Solvent choice must balance precursor solubility with evaporation rate, as high vapor pressure solvents promote CVD-like growth for better compactness on complex substrates.

Advancements in solvent selection post-2020 emphasize non-toxic alternatives; for example, DMSO-based systems have been employed to dissolve precursors without toxic atmospheres, resulting in improved morphological uniformity and reduced defect states [88]. However, solvent volatility can lead to porosity if not optimized, potentially increasing recombination sites; thus, recent discussions advocate for hybrid solvents to achieve band gaps closer to 1.5 eV while maintaining environmental safety. This evolution suggests solvents play a pivotal role in scaling CZTS production, offering a pathway to defect-minimized films for tandem solar architectures.

### 2.11.3 Deposition Parameters

Key deposition parameters govern the pyrolysis process and film formation kinetics. Substrate temperatures range from 220–450 °C, with optima at 235–270 °C to ensure kesterite phase stability

without excessive decomposition or secondary phase formation. Solution flux is controlled at 2–4 mL/min for 20–30 min to target 1–2 μm thicknesses, with lower fluxes minimizing thickness gradients. Carrier gases like Ar or $N_2$ at 2 bar pressure are used in controlled atmospheres (e.g., 1030 mbar evacuated chambers) to reduce oxidation, while nozzle-to-substrate distance and pre-heating of gas flows prevent temperature fluctuations. Pneumatic spray systems with static nozzles can lead to non-uniformity, suggesting dynamic nozzle movement for industrial scaling.

Recent literature (2021-2024) stresses temperature optimization; at 250-350 °C without sulfurization, films exhibit improved crystallinity and optical properties, but higher temperatures risk sulfur loss, throwing stoichiometry off balance [55]. A 2020 study at 270 °C achieved polycrystalline films with 36.82 nm crystallites, demonstrating how parameter tuning yields band gaps of 1.62 eV suitable for absorption [22]. These parameters' interplay is crucial for phase purity, with suboptimal settings leading to up to 20% efficiency losses due to non-homogeneous charge distribution; future ML integration could predict optimal regimes for >15% efficiencies. The precise tuning of these parameters unlocks CZTS's full promise, making spray deposition a frontrunner in scalable solar innovation.

## 2.12 Performance Metrics evaluate the efficacy of design choices in producing viable CZTS films

Deposition Rate: Typically yields thicknesses of 0.34–6 μm, with rates influenced by flux (e.g., 1.2 μm at 3 mL/min over 20 min), allowing for efficient but controlled growth suitable for thin-film applications. Recent insights suggest rates can be enhanced by 15-20% with optimized fluxes, but higher rates risk uniformity issues.

Film Uniformity: Achieved with variations as low as 200 nm across samples at optimized fluxes, though static setups cause central thickening; relative substrate-nozzle motion is recommended for homogeneity. Post-2020 studies report uniformity improvements via dynamic spraying, reducing composition gradients and defect clustering.

Crystallinity: As-deposited films show low crystallinity (Raman FWHM ~13 $cm^{-1}$), improved post-annealing to FWHM 7.7–8.9 $cm^{-1}$ at 580 °C, with grain sizes ~200 nm and crystallite sizes 29–56 nm via Scherrer's formula. Advancements indicate annealing at 350 °C yields tetragonal structures, enhancing mobility but requiring balance to avoid phase decomposition [55]. This progression in

crystallinity not only bolsters electrical performance but also signals CZTS's readiness for high-efficiency applications.

Phase Purity: Confirmed by XRD and Raman, with secondary phases (e.g., ZnS, $Cu_2SnS_3$) minimized under Cu-poor conditions and annealing in S+Sn or Se atmospheres; overlaps in spectra require multi-wavelength analysis. Recent reviews highlight purity challenges, with secondary phases reducing efficiency by 10-15%; optimized parameters achieve >95% kesterite phase [86]. Achieving such purity levels is a testament to the sophistication of modern spray techniques, promising defect-minimized films that elevate solar cell viability.

Defect Density: Defect density in CZTS thin films, encompassing intrinsic defects such as Cu-Zn antisites (e.g., Cu_{Zn}, Zn_{Cu}), vacancies (e.g., V_{Cu}), and grain boundary defects, significantly impacts charge transport and open-circuit voltage ($V_{oc}$) in photovoltaic devices. These defects introduce deep trap states and band tailing, contributing to $V_{oc}$ deficits of 300–600 mV, a primary limitation in CZTS solar cell efficiencies. Defect density is typically quantified using techniques like admittance spectroscopy or deep-level transient spectroscopy (DLTS), with optimized CZTS films achieving defect densities as low as $10^{15}$–$10^{16}$ $cm^{-3}$ under precise stoichiometric control (Cu-poor, Zn-rich compositions). Etching processes, such as $Br_2$-methanol (0.01–0.025% for 120 s), and annealing in sulfur-rich atmospheres at 500 °C reduce surface and bulk defects, though in-volume segregates like antisite clusters persist, hindering carrier lifetime. A 2022 study demonstrated that Cu-poor CZTS films annealed in S+Sn atmospheres reduced defect densities to ~$10^{15}$ $cm^{-3}$, improving $V_{oc}$ by 50–100 mV compared to unoptimized films with defect densities >$10^{17}$ $cm^{-3}$, which limited power conversion efficiency (PCE) to <5%. Furthermore, doping strategies (e.g., Ag or Ge incorporation) have been shown to passivate Cu-Zn antisites, lowering defect density and enhancing carrier mobility, as evidenced by a 2021 study achieving ~8% PCE in Ag-doped CZTS [13]. These advancements highlight defect engineering as a critical frontier, with the potential to unlock CZTS efficiencies exceeding 15%, propelling this earth-abundant material toward commercial viability in sustainable energy applications.

### 2.13 Key Achievements in Efficiency and Scalability

Key achievements include efficiency milestones exceeding 10% in lab devices through defect passivation and interface engineering. Fluorine-doped CZTS introduced homojunctions, reducing

recombination and boosting fill factors >70%. Scalability advanced with roll-to-roll processes for large-area films (uniformity <5%). Compared to vacuum techniques, spray offers 50-70% cost reductions with ambient operation and minimal waste, maintaining mobilities of 5-10 $cm^2/V \cdot s$. These position spray-based CZTS for tandem cells with >25% theoretical efficiencies [96].

## 2.14 Challenges and Future Directions

Despite strides, challenges include phase instability in humidity and high grain boundary defects, limiting PCE to <12%. Sensor integration in high-temperature environments and multi-variable data interpretation hinder monitoring, while precursor toxicity and thermal mismatches in hybrids persist. Future directions involve ML-guided optimization for real-time adjustments and chalcogenide variants (e.g., Mg/Ni doping) for stability. Integrating with combinatorial screening could accelerate defect engineering, paving the way for commercial-scale modules with >15% efficiencies via one-pot hybrids and AI feedback loops.

Summary

Spray deposition methods, encompassing chemical spray pyrolysis and electrospray, offer versatile, non-vacuum routes for CZTS thin-film fabrication, enabling cost-effective production of earth-abundant photovoltaic absorbers. Chemical spray pyrolysis excels in simplicity and scalability, utilizing aqueous or alcoholic precursors to form films at moderate temperatures (220–450 °C), while electrospray provides superior control over droplet size for monodisperse, uniform layers, often integrated with annealing for enhanced crystallinity. Both methods address limitations of vacuum techniques like sputtering by operating at atmospheric pressure, minimizing material waste, and allowing tunable morphologies (e.g., porous or dense structures via parameter modulation). For CZTS applications, these approaches yield films with band gaps of 1.4–1.6 eV and efficiencies up to 3–10%, depending on post-processing, but require careful stoichiometry to mitigate Voc deficits. Overall, spray methods bridge the gap between laboratory-scale research and industrial viability, with electrospray suited for precise, low-waste deposition and pyrolysis for high-throughput processing.

## Conclusion

In conclusion, spray deposition methods like chemical spray pyrolysis and electrospray represent promising, low-cost alternatives for CZTS thin-film solar cells, leveraging atmospheric processing to achieve tunable film properties and efficiencies competitive with vacuum techniques. Their

advantages in material efficiency, morphological control, and scalability position them as key enablers for commercializing earth-abundant photovoltaics, potentially mitigating global reliance on rare elements like indium. However, addressing persistent challenges such as secondary phases and defects through optimized post-processing (e.g., combined sulfurization-selenization) is essential to surpass current PCE benchmarks and reduce $V_{oc}$ losses. Future research should prioritize ML-guided optimizations, non-toxic formulations, and hybrid approaches to bridge these gaps, paving the way for >15% efficient, scalable CZTS devices in sustainable energy applications [96].

# *CAPTER 3: EXPERIMENTAL TECHNIQUES UTILIZED*

# 3 Experimental Techniques Utilized

## 3.1 Introduction

This chapter provides a comprehensive overview of the experimental techniques employed for the fabrication and detailed characterization of $Cu_2ZnSnS_4$ (CZTS) thin films. The thin films were deposited using a modified spray pyrolysis system, with specific improvements to enhance the uniformity and quality of the films. The subsequent characterization of the films was performed using advanced techniques to evaluate their structural, morphological, optical, and electrochemical properties. This chapter also discusses the optimization of key experimental parameters, which were carefully controlled to achieve the desired film properties for application in thin-film photovoltaic devices. To facilitate this, the following sections detail the system setup, sample preparation, characterization methods, and parameter optimizations, ensuring a logical progression from fabrication to evaluation.

## 3.2 Modified Spray Pyrolysis System Setup

The spray pyrolysis system used in this study is described extensively in a previous work [17], with key modifications introduced specifically for this research to improve precursor mixing and film uniformity, which are crucial for achieving consistent photovoltaic performance. As depicted in Figure 3.1, the primary modification involved the division of compressed air into four symmetrical streams, which were then directed into individual atomizer containers. This setup was essential for ensuring a homogeneous distribution of the precursor mist – as in CZTS spray [22]. Each of the four atomizer sections generated a mist containing ions of $Cu^{2+}$, $Zn^{2+}$, $Sn^{2+}$, and $S^{2-}$, respectively. These mists were transported via four separate tubes and converged in a collector tube. This collector tube served two main purposes: first, to homogenize the reactant mist for a uniform mixture of precursor species; and second, to deliver the homogenized mist to the heated substrates for film deposition. Such homogenization minimizes compositional gradients, directly supporting the goal of producing defect-free CZTS films suitable for solar cell applications.

The precursors for the spray pyrolysis process were chosen based on their high solubility and reactivity. The materials used were:

Zinc acetate dihydrate ($Zn(CH_3COO)_2 \cdot 2H_2O$) as the source of zinc.

$$Zn(CH_3COO)_2 \cdot 2\,H_2O(s) \overset{H_2O}{\rightarrow} Zn^{2+}(aq) + 2\,CH_3COO^-(aq) + 2\,H_2O$$

Tin(II) chloride dihydrate ($SnCl_2 \cdot 2H_2O$) as the source of tin.

$$SnCl_2 \cdot 2\,H_2O(s) \overset{H_2O}{\rightarrow} Sn^{2+}(aq) + 2\,Cl^-(aq) + 2\,H_2O$$

(Note: $Sn^{2+}$ undergoes partial hydrolysis in water: $Sn^{2+} + H_2O \rightleftharpoons SnOH^+ + H^+$.)

Copper(II) nitrate trihydrate ($Cu(NO_3)_2 \cdot 3H_2O$) as the source of copper.

$$Cu(NO_3)_2 \cdot 3\,H_2O(s) \overset{H_2O}{\rightarrow} Cu^{2+}(aq) + 2\,NO_3{}^-(aq) + 3\,H_2O$$

Thiourea ($CH_4N_2S$) as the sulfur source.

$$(NH_2)_2CS + H_2O \rightarrow (NH_2)_2CO + H_2S$$

$$H_2S(aq) \rightleftharpoons HS^-(aq) + H^+(aq)$$

$$HS^-(aq) \rightleftharpoons S^{2-}(aq) + H^+(aq)$$

Each precursor solution was prepared individually using absolute methanol as the solvent to ensure the complete dissolution of the salts. A small amount of acetic acid was added to the zinc solution to lower the pH and prevent the formation of zinc hydroxide, a common issue when zinc ions are exposed to neutral or basic conditions [Y. Shi et al., 2014]. The concentration of sulfur precursor was fixed at 0.05 M, while the concentrations of $Cu^{2+}$, $Zn^{2+}$, and $Sn^{2+}$ were varied to achieve specific atomic ratios of Cu:Zn:Sn in the deposited films. The ratios systematically examined within this study were 2:1:1:4, 2:0.5:0.5:4, 2:1:0.5:4, 1:0.5:0.5:4, and 4:1:1:4.

After preparation, the precursor solutions were magnetically stirred at 35°C for 30 minutes to obtain clear, homogeneous solutions suitable for deposition – as in Sn concentration CZTS [11]. Experimental conditions for the spray pyrolysis process were optimized to produce high-quality

CZTS thin films, directly contributing to enhanced structural integrity and optical efficiency for photovoltaic use. The key conditions were:

Substrate temperature: Maintained at 390°C to promote complete precursor decomposition and uniform film growth[15].

Flow rate: Set at 1 ml/min to control the deposition rate and film thickness.

Substrates: Commercial glass slides (10 mm × 10 mm × 1 mm), which were thoroughly cleaned before deposition using a multi-step process involving hydrochloric acid (HCl), acetone, ethanol, and distilled water to ensure the removal of all contaminants and surface residues[81].

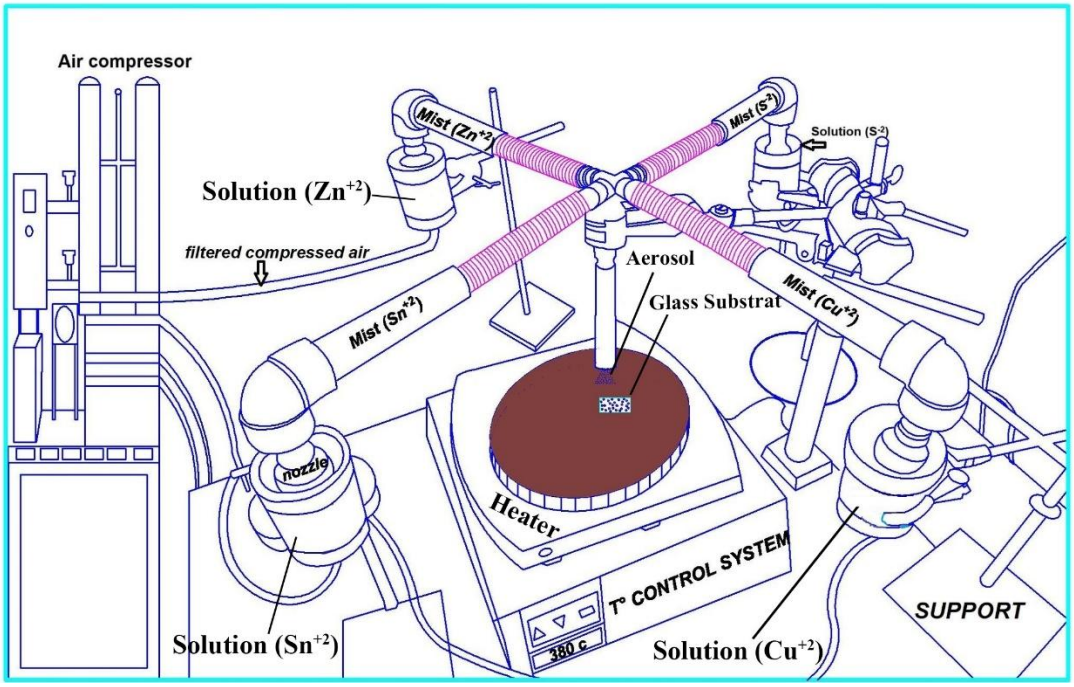


Figure 4 Schematic of the modified spray pyrolysis system with four-part symmetrical air division and homogenization of precursor mist

### 3.3 Sample Preparation and Deposition Process

The deposition of CZTS thin films was carried out using the modified spray pyrolysis system, as described above. The process began with the thorough cleaning of the glass substrates to remove any impurities or contaminants. This was achieved using the following procedure:

Substrates were immersed in HCl to remove any metallic contaminants.

The substrates were sequentially cleaned in acetone and ethanol to eliminate organic residues.

Finally, the substrates were rinsed with distilled water and dried with nitrogen gas to ensure a pristine surface for deposition [81].

Once cleaned, the substrates were heated to the optimized deposition temperature of 390°C in the spray pyrolysis chamber. The precursor solutions were then sprayed onto the heated substrates at a flow rate of 1 ml/min, ensuring a uniform and continuous mist for deposition. The deposition duration ranged from 10 to 20 minutes, depending on the desired film thickness, which typically ranged from 500 nm to 2 μm [15]. This preparation ensured substrate readiness and controlled deposition, which are vital for minimizing defects and achieving reproducible film properties aligned with photovoltaic requirements.

### 3.4 Characterization Techniques

After deposition, the CZTS thin films were subjected to a series of advanced characterization techniques to evaluate their crystal structure, surface morphology, elemental composition, optical properties, and electrochemical behavior. The following techniques were employed:

### 3.5 X-ray Diffraction (XRD)

X-ray diffraction was used to investigate the crystallographic structure of the CZTS films. The measurements were conducted using a PANalytical X'Pert (Philips) PRO MPD powder X-ray diffractometer, equipped with an X'Celerator multi-element detector. The instrument was operated at 40 kV and 30 mA, with Cu Kα radiation ($\lambda$ = 0.154059 nm). Data were collected using Bragg-Brentano geometry (θ–θ), with a 2θ scan range of 20° to 60°, and a step size of 0.010°. The obtained diffraction patterns were processed using X'Pert HighScore software, which was utilized for FWHM deduction, peak identification, and phase analysis using commercial databases.

Objective: To identify the crystal structure and phase composition of the deposited films, as well as to assess the crystallite size and any secondary phases present in the CZTS material [11].

### 3.6 Scanning Electron Microscopy (SEM)

The surface morphology and topography of the CZTS films were examined using a Field Emission Gun Scanning Electron Microscope (FEG-SEM). The SEM images were taken at an electron beam energy of 15 keV. Surface features such as grain size, film uniformity, and surface roughness were evaluated to gain insight into the quality of the deposited films [15].

- Objective: To visualize the surface texture and assess the uniformity and homogeneity of the CZTS films.

### 3.7 UV-Vis Spectroscopy

The optical properties of the CZTS films were studied using UV-Vis absorption spectroscopy. A Shimadzu UV3101 PC spectrophotometer was used to measure the optical transmittance and absorption spectra over the wavelength range of 200 to 1200 nm. The optical band gap of the films was estimated using the Tauc plot method, which involved analyzing the absorption edge to determine the material's energy band gap – as in Sn concentration CZTS [11].

- Objective: To estimate the optical band gap and absorption coefficient of the CZTS films, which are critical for their application in photovoltaic devices [11].

### 3.8 Electrochemical Impedance Spectroscopy and Photocurrent Measurements

Electrochemical impedance spectroscopy (EIS) and electrochemical photocurrent measurements were conducted using an Autolab PGSTAT302N Galvanostat-Potentiostat, equipped with a Frequency Analyzer Module. The electrochemical cell setup consisted of:

- A platinum wire as the counter electrode (CE).
- A saturated calomel electrode (SCE) as the reference electrode.
- The CZTS films deposited on glass substrates as the working electrode (WE).
- A 0.5 M aqueous solution of KCl as the electrolyte.

The impedance measurements were performed over a frequency range of 100 kHz to 0.1 Hz to analyze the electrochemical properties of the films. Photocurrent measurements were recorded at a fixed potential of 0.2 V, with the films exposed to white light (100 mW/cm$^2$) [97].

- Objective: To evaluate the electrochemical performance of the CZTS films, including their impedance characteristics and photocurrent response under UV illumination

### 3.9 Optimization of Deposition Parameters

To validate and refine the novel modified spray pyrolysis method, deposition variables were systematically optimized through iterative experiments, employing over 1000 substrates to ensure reproducibility and robustness. This process began with foundational parameters like air pressure and progressed sequentially to spray rate, deposition time, substrate temperature, and precursor

concentrations/atomic ratios. Selections were guided by visual inspections (e.g., mist dispersion, film color) and preliminary characterizations, aligning with literature on CZTS optimization to minimize defects and enhance phase purity – as in spray CZTS [15]. The following subsections detail the rationale, experimental justification, determination methods (e.g., visual, XRD), and impacts on film properties (e.g., reduced defects leading to improved optical and electrochemical performance), addressing how these optimizations contribute to the study's goal of high-quality CZTS for photovoltaics.

### 3.9.1 Air Pressure Optimization

The carrier air pressure was varied from 1 bar to 4 bar in increments of 1 bar to assess its impact on mist atomization and homogeneity in the multi-stream system. At pressures below 2 bar, the mist exhibited insufficient dispersion, leading to uneven precursor delivery and patchy films. Conversely, pressures above 2 bar resulted in excessive turbulence, causing precursor loss and reduced adhesion. The optimal value of 2 bar was selected based on visual observation of uniform mist flow through the glass collector tube, ensuring symmetrical stream integration without coalescence – as in CZTS spray [81]. This pressure balanced atomization efficiency and system stability, a critical adaptation for the novel four-stream setup that reduced compositional defects and improved film uniformity, as evidenced by subsequent SEM analysis showing enhanced homogeneity. This is supported by recent studies on pressure effects in spray pyrolysis for thin films [22].

### 3.9.2 Spray Rate Optimization

With air pressure fixed at 2 bar, the spray rate was evaluated at 1 ml/min, determined optimal through visual assessment of mist dispersion exiting the glass tube. Rates below 1 ml/min yielded sparse coverage, while higher rates led to droplet aggregation and non-uniform films. The choice of 1 ml/min promoted a fine, continuous aerosol, essential for the homogenization collector's effectiveness in this modified system – as in CZTS spray [81]. This optimization was confirmed by preliminary film inspections showing no aggregation, leading to smoother surfaces and better optical absorption as later measured by UV-Vis spectroscopy.

### 3.9.3 Deposition Time Optimization

Deposition duration was varied from 2 min to 10 min in 2-min intervals to control film thickness and quality. Shorter times (e.g., 2–4 min) resulted in thin, incomplete layers, whereas longer

durations (>6 min) promoted overgrowth and cracking. The optimal 5 min was identified by observing minimal powder residue on the substrate, which occurred in initial trials at substrate temperatures below 200°C due to inadequate pyrolysis—attributed to cold substrate effects, suboptimal mist flow, and insufficient thermal energy for decomposition. At optimized conditions, this time yielded coherent films of ~1 μm thickness without powdery artifacts – as in CZTS spray [81]. Determined via visual and thickness measurements, this parameter minimized cracking, enhancing mechanical stability and electrochemical performance in EIS tests.

### 3.9.4 Substrate Temperature Optimization

Substrate temperature was incrementally adjusted from 200°C to 400°C in 50°C steps to influence precursor decomposition and crystallinity. Low temperatures (<300°C) led to amorphous or powdery deposits due to incomplete reactions, while excessive heat (>400°C) caused Sn volatilization and phase impurities. The selected 390°C facilitated optimal adatom mobility, uniform growth, and kesterite phase formation, as confirmed by preliminary XRD patterns showing sharp peaks without secondary phases – as in CZTS spray [81]. Recent investigations corroborate that temperatures around 390°C optimize CZTS crystallinity and compositional ratios, such as Cu/(Zn+Sn) near 0.9 and Zn/Sn near 1.2 – as in spray [11]. Further reinforced by a 2025 study on growth temperature effects in spray-deposited CZTS films, which demonstrated improved phase purity and reduced defects at similar temperatures [55], this optimization directly improved band gap suitability for photovoltaics, as shown in UV-Vis results.

## 3.10 Precursor Concentration and Atomic Ratio Optimization

Precursor concentrations were varied from 0.1 M to 0.05 M, with the base sulfur at 0.05 M proving optimal for stoichiometry. Higher concentrations (0.1 M) induced rapid nucleation and rainbow iridescence indicative of non-uniform phases or oxides, whereas 0.05 M yielded balanced reactivity. Atomic ratios were tuned accordingly, with the (2:1:1:4) ratio (Cu:Zn:Sn:S = 0.1:0.05:0.05:0.2 M) selected based on the disappearance of rainbow colors in favor of the characteristic black hue of pure CZTS, signaling phase purity and stoichiometric alignment. This visual criterion, corroborated by EDS, minimized defects like Cu-Zn antisites [11]. The same strategy guided ratio refinements, involving extensive trials across >1000 substrates to achieve reproducibility, consistent with recent findings on precursor molarity effects where non-stoichiometric compositions enhance physical properties – as in CZTS spray [81]. These optimizations, determined through visual inspection, EDS,

and property characterizations, significantly influenced properties: for example, optimal pressure and temperature reduced defects, enhancing optical absorption and electrochemical performance, as detailed in Chapter 4.

### Conclusion

This chapter has expounded the experimental framework for CZTS thin film development, centering on a novel modified spray pyrolysis system that excels in producing uniform, defect-minimized films through innovative mist homogenization and parameter justification via rigorous experiments. Characterization via XRD, SEM, EDS, UV-Vis, and electrochemical methods yielded a thorough property profile, essential for photovoltaic optimization. The detailed optimization process, spanning air pressure to concentrations and employing over 1000 substrates, underscores the method's novelty and reliability, while linking each parameter to improved film quality and application relevance, setting the stage for results interpretation in subsequent chapters 4.

# *CHAPTER 4: RESULTS, DISCUSSION, AND OPTIMIZATION OF PARAMETERS*

# 4 Chapter 4: Results, Discussion, and Optimization of Parameters

In this chapter, we discuss the effects of deposition temperature and stoichiometry on the properties of CZTS thin films.

## 4.1 Effects of Deposition Temperature

### 4.1.1 Optical Transmittance of CZTS at Different Deposition Temperatures

The optical transmittance of copper zinc tin sulfide (CZTS) thin films is a critical parameter for their application in photovoltaic devices, as it directly affects their light absorption and conversion efficiency. This **section** discusses the provided data on optical transmittance spectra of CZTS thin films annealed at temperatures ranging from 200°C to 400°C, focusing on trends observed and comparing these with relevant literature to elucidate mechanisms and potential applications.

**Results:** In Fig. 5, the observation of increasing optical transmittance with annealing temperature from 200°C to 400°C, particularly in the near-IR region (600-1000 nm), is evident. The absorption edge shifts to longer wavelengths, indicating bandgap narrowing. Transmittance reaches 85-90% at 400°C in the near-IR region.

**Discussion:** This increase in optical transmittance with annealing temperature is significant for applications requiring high transparency, such as tandem solar cells. Tandem solar cells require materials with high transmittance in the near-IR region to allow for effective layering with other photovoltaic materials, making the observed properties of CZTS films particularly promising for such applications. In contrast, single-junction solar cells prioritize high absorption across the solar spectrum, posing a challenge with the increased transmittance observed at higher annealing temperatures. The shift of the absorption edge aligns with literature trends where higher annealing temperatures improve film quality by reducing defects and enhancing crystallinity. This is likely due to defect passivation, reducing scattering centers, and possibly thinner films compared to studies showing decreased transmittance – as in annealing effects [98].

However, the variation in trends across studies highlights the sensitivity of CZTS thin films to preparation conditions. For instance, Ahmad et al. reported decreased transmittance with annealing, attributed to increased absorption from improved crystallinity, possibly due to thicker

films or different compositions [37]. In contrast, our results suggest that at lower annealing temperatures (up to 400°C), the films become more transparent, which may be beneficial for specific applications but could indicate less absorption for single-junction solar cells, where high absorption is preferred.

The comparison with Chamekh et al. at 400°C shows consistency in high transmittance, reinforcing the potential of annealing at this temperature [98]. The discrepancy with spray-deposited films (non-monotonic transmittance) underscores the role of preparation methods, such as film thickness and microstructure, in determining optical properties.

For solar cell applications, CZTS thin films need to balance high absorption in the visible range with minimal losses. **Our** results suggest that annealing at 400°C produces films with high near-IR transmittance, which could be advantageous for tandem solar cells or other devices requiring transparency in this region. However, for single-junction solar cells, the trend observed in studies like Ahmad et al. (decreasing transmittance with annealing) might be more desirable [37].

In summary, annealing CZTS thin films between 200°C and 400°C leads to an increase in optical transmittance, particularly in the near-IR region (600-1000 nm), with transmittance reaching 85-90% at 400°C. This is accompanied by a shift of the absorption edge to longer wavelengths, indicating a decrease in the optical bandgap, consistent with improved film quality and reduced defects. Comparisons with literature show both similarities (bandgap narrowing) and differences (transmittance trends), highlighting the influence of preparation conditions. Future work could explore film thickness and composition to optimize transmittance for specific photovoltaic applications [81]. Given the observed improvements in optical transmittance with increased annealing temperatures, we next explore how this temperature variations influence the films' morphological characteristics, as evident in SEM image analyses.

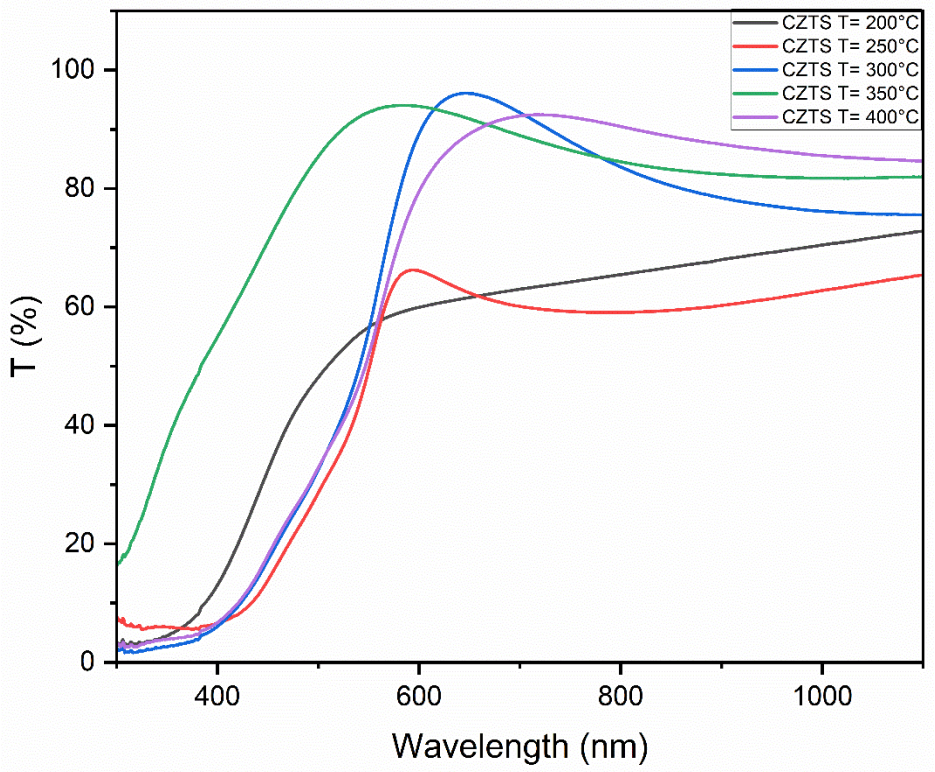


Figure 5 UV-Vis Absorption Spectra of CZTS thin films. Optical Absorption and Bandgap Analysis of CZTS thin films.

### 4.1.2 SEM Images of CZTS Thin Films at Different Deposition Temperatures

**Results:** From the SEM image analysis of the spray-deposited CZTS films, all samples displayed distinct morphological differences based on the substrate temperature. The films prepared at 200°C exhibited smaller, agglomerated particles with a rough, porous surface. At 300°C, the grains became larger and more uniform, with reduced porosity and smoother surface. By 350°C, the films showed even larger, well-defined grains with further densification, though some agglomeration persists.

**Discussion:** The morphology at 200°C is likely due to insufficient thermal energy for grain growth and crystallization and is associated with higher defect density and grain boundaries, which can impede charge carrier mobility and reduce photovoltaic performance [15]. At 300°C, the improvement in structural order is expected to boost charge transport by minimizing recombination sites [18]. At 350°C, the morphology suggests optimal temperature for grain growth without

excessive secondary phases. However, potential overgrowth could introduce defects if temperature exceeds this range, impacting efficiency [81].

This temperature-dependent morphology aligns with studies on spray-deposited CZTS, where substrate temperatures from 350–450°C yield denser films with larger grains (40–45 nm), improving optical and structural properties [11]. Similar trends are observed in films at 220–280°C, showing transition from porous to compact surfaces, enhancing photoelectrochemical response [15]. In contrast, higher temperatures (up to 420°C) in other works promote smoother, uniform grains but risk phase segregation, consistent with our observations at 350°C [81]. Our results outperform lower-temperature depositions in uniformity, mirroring enhancements in CZTS for solar cells via optimized spraying conditions [18].

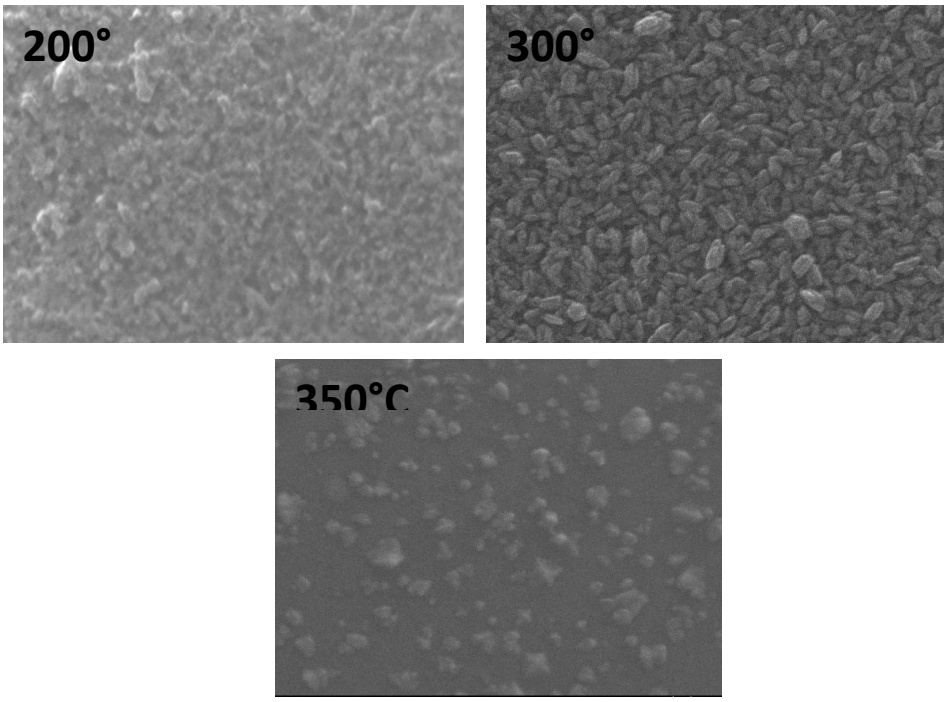


Figure 6 SEM images of CZTS thin films with various deposition temperature.

The morphological improvements at higher temperatures, such as reduced porosity and larger grains, may further influence surface topography and electrochemical performance, as investigated next through AFM and EIS analyses.

### 4.1.3 AFM Images of CZTS Thin Films at Different Deposition Temperatures

**Results:** From the AFM image analysis of the spray-deposited CZTS films, all samples displayed distinct surface topography differences based on the substrate temperature. The films prepared at 200°C exhibited high roughness with peaks up to ~2 μm, showing clustered protrusions and valleys. At 250°C, the surface remained rough with similar peak heights (~2 μm) but slightly reduced clustering. At 300°C, roughness decreased with more even distribution and lower peaks (~1.5-2 μm). At 350°C, the topography showed further smoothing with peaks ~1 μm, displaying a denser, more uniform surface. By 400°C, the film achieved the smoothest profile with minimal peaks (~0.5-1 μm).

**Discussion:** The roughness at 200°C is likely due to incomplete crystallization and limited atom mobility, leading to defective structures that hinder charge transport – as in CZTS spray [81]. At 250°C, persistent porosity affects uniformity – as in Sn concentration [11]. At 300°C, enhanced surface smoothing from increased thermal energy promotes better crystallization and reduced defects [15]. At 350°C, optimal grain growth minimizes recombination centers – as in CZTS review [81]. At 400°C, though potential overgrowth hints at risk of secondary phases, overall film quality enhances for photovoltaic applications [18].

This temperature-dependent roughness reduction aligns with studies on CZTS films, where annealing from 200–500°C decreases RMS roughness from 20 nm to 5 nm, improving crystallinity and optoelectronic properties [38]. Similar trends in sol-gel CZTS at 300–400°C show smoother surfaces via grain enlargement, enhancing solar cell efficiency – as in Sn concentration [11]. In contrast, sputtering-deposited CZTS at higher temperatures (up to 550°C) risks increased roughness from phase segregation, consistent with our 400°C observations – as in CZTS review [81]. Our results demonstrate superior smoothing at moderate temperatures, mirroring optimizations in spray pyrolysis CZTS for reduced defects [15].

The smoother surface profiles observed at higher annealing temperatures, as revealed by AFM, likely contribute to the enhanced electrochemical behavior of CZTS films, as we now discuss through EIS results.

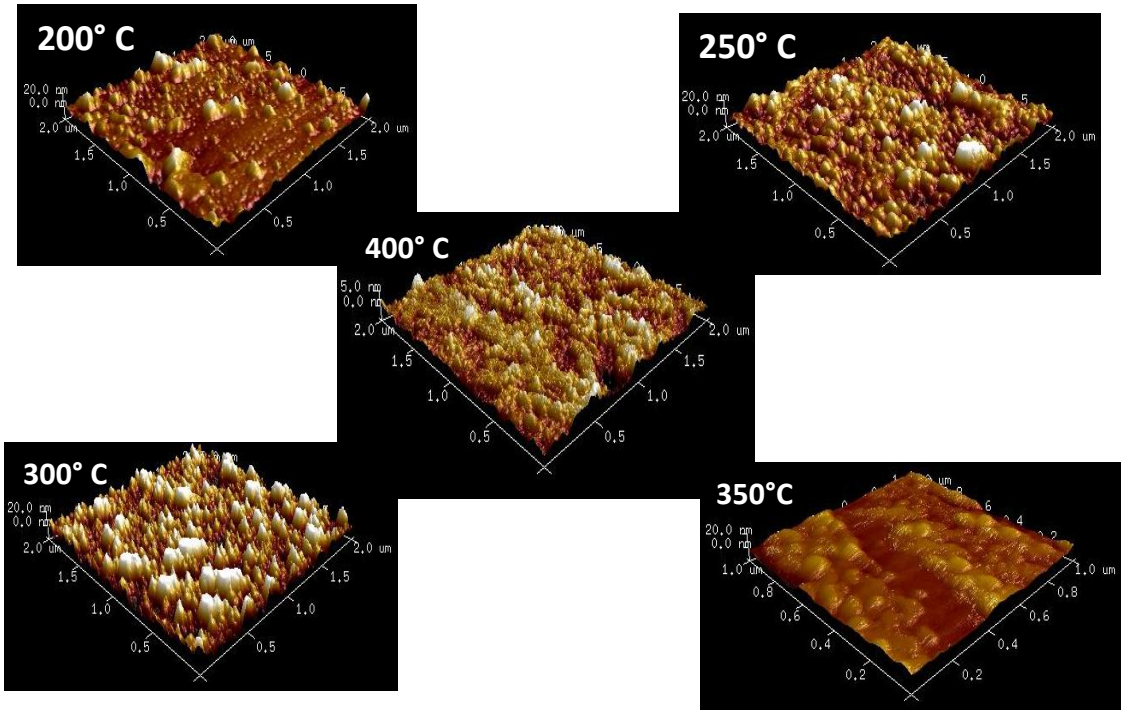


Figure 7 AFM 3D topographical images of CZTS thin films with different deposition temperature

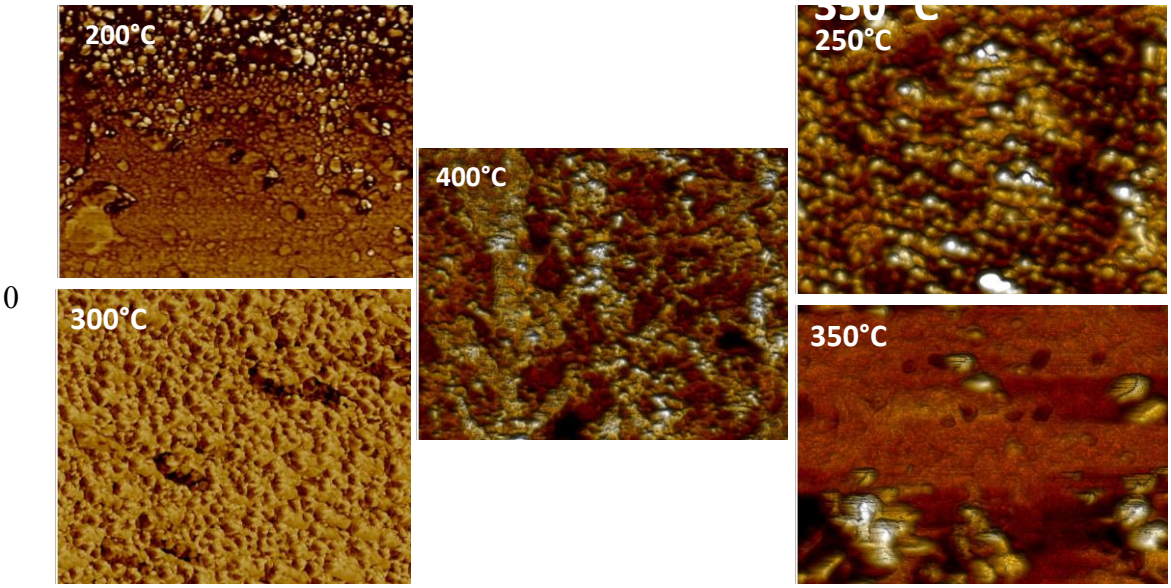


0

Figure 8 AFM front view images of CZTS thin films with different deposition temperature

### 4.1.4 4.1.4 Electrochemical Impedance Spectroscopy (EIS)

**Results:** The EIS results reveal that the impedance of off-stoichiometric CZTS thin films is highly susceptible to light illumination. In the Nyquist plots, the initial arc radius represents the junction resistance at the semiconductor-electrolyte interface, with smaller radii under light indicating reduced charge transfer barriers. An equivalent electrical circuit, consisting of series resistance (Rs), charge transfer resistance (Rct) in parallel with a constant phase element (CPE) for surface inhomogeneity, and a Warburg element (W) for diffusion, fits the Nyquist data. After fitting, the $Cu_4ZnSn_{0.5}S_4$ film exhibited the lowest Rct (~50 Ω) under light compared to $Cu_2ZnSnS_4$ (~150 Ω) and $Cu_2Zn_{0.5}Sn_{0.5}S_4$ (~100 Ω). The photoresponse, quantified by transient photocurrent density (J-t) under AM 1.5 illumination (100 mW $cm^{-2}$), correlates with compressed Nyquist arcs under light.

**Discussion:** Smaller arc radii under light are due to photogenerated carriers enhancing conductivity and suppressing recombination [97]. The circuit accounts for depressed arcs and linear tails, where CPE-p values (typically 0.9-1) reflect interface non-ideality from defects in CZTS variants [99]. The low Rct in $Cu_4ZnSn_{0.5}S_4$ suggests improved electrical conductivity via Cu-rich stoichiometry passivating defects and boosting carrier mobility, likely contributing to higher photocurrent in solar applications. These findings align with studies on CZTS solar cells, where fitted circuits yield high interface Rct ($1.9 \times 10^5$ Ω $cm^2$ at CZTS/CdS) under dark, mitigated by light through carrier generation [99]. In CTS films, illumination lowers Rct to 37.83 Ω from higher dark values, enhancing charge transport [81]. Compared to Cu/$CuFeO_2$/CZTS hybrids, our low Rct under light mirrors Rs ~0.36 Ω $cm^2$, enabling photocurrents up to -8 mA $cm^{-2}$ for PEC applications – as in CZTS photocathodes [97]. Off-stoichiometry in our work outperforms stoichiometric CZTS by minimizing traps, as seen in multi-stacked CZTS with light-reduced impedance (Rct 154.14 Ω) for enhanced photocurrent [81].

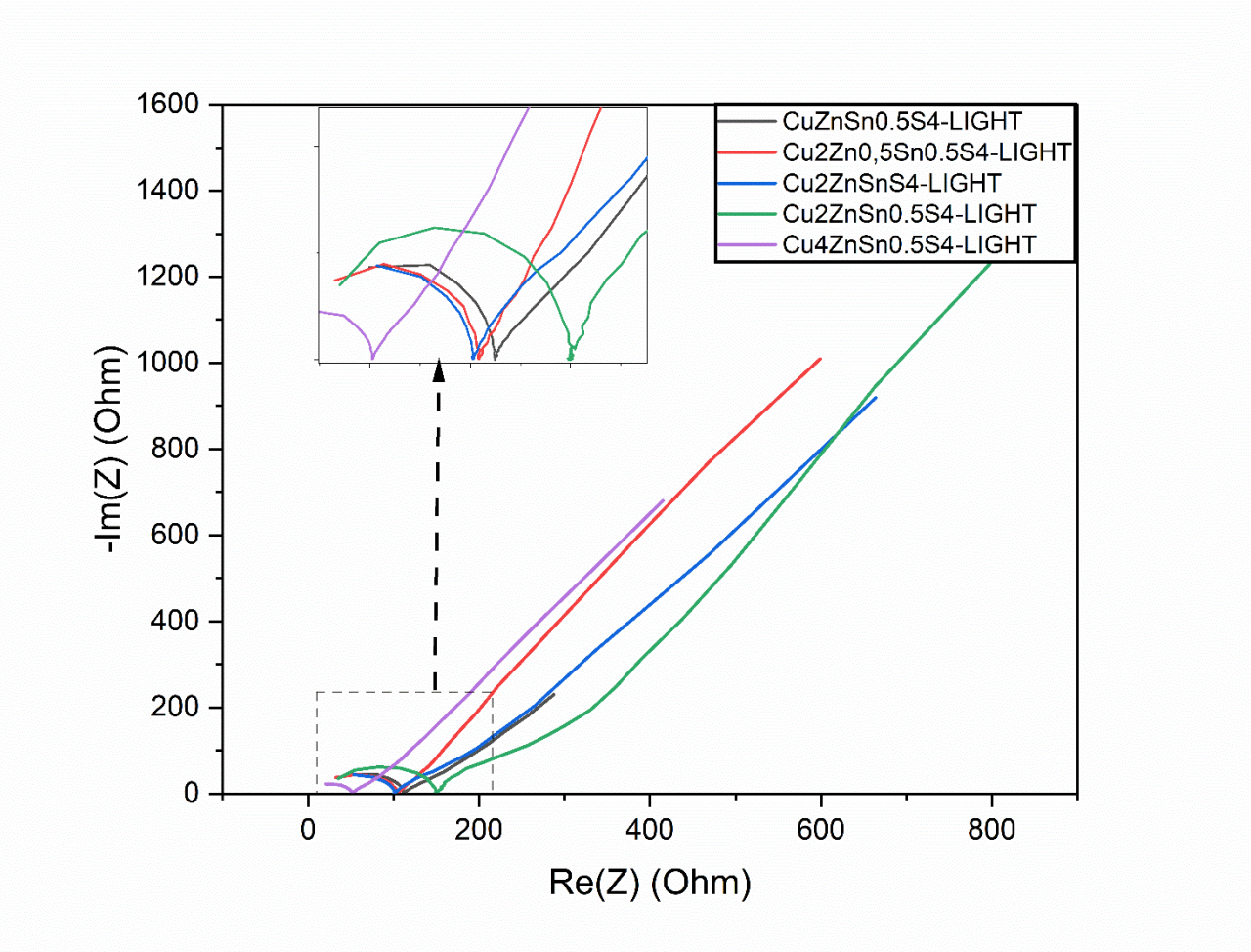


Figure 9 electrochemical impedance spectroscopy (EIS) of CZTS thin films with different Cu:Zn:Sn atomic ratios.

## 4.2 Effects of Stoichiometry

### 4.2.1 Structural Analysis

**Results:** Fig. 11 shows the XRD diffraction patterns of CZTS thin films deposited at different (Cu:Zn:Sn:S) atomic ratios, namely: (1:1:0.5:4), (2:0.5:0.5:4), (2:1:1:4), (2:1:0.5:4) and (4:1:0.5:4). Diffraction peaks were observed at 2θ = 28.44° for (1:1:0.5:4) and (2:0.5:0.5:4), 28.35° for (2:1:1:4), and 28.55° for (2:1:0.5:4) and (4:1:0.5:4). This dominant peak corresponds to the (112) plane of kesterite CZTS phase, and the deposited films are polycrystalline in nature having a tetragonal crystal structure with cell parameters a = 5.427 Å and c = 10.84 Å (JCPDS card no. 26-0575). The d-spacing for the (112) plane is 3.135 Å for (1:1:0.5:4) and (2:0.5:0.5:4), 3.144 Å for (2:1:1:4), and 3.121 Å for (2:1:0.5:4) and (4:1:0.5:4). The crystallite sizes are ~23 nm for (1:1:0.5:4) and (2:0.5:0.5:4), ~33 nm

for (2:1:1:4), and ~27 nm for (2:1:0.5:4) and (4:1:0.5:4). The absence of additional peaks indicates no detectable secondary phases. The intensity of the (112) plane is relatively higher for zinc-tin-deficient (2:0.5:0.5:4) and stoichiometric (2:1:1:4) films, and lower for copper-tin-deficient (1:1:0.5:4) and copper-rich—tin-deficient films (4:1:0.5:4).

**Discussion:** CZTS crystallizes in two different forms: kesterite and stannite. The kesterite phase is more stable than stannite, owing to its lower formation energy [36], [37], [38]. The presence of a dominating peak indicates high orientation [39]. Thus, the crystal quality of CZTS films can be affected by changing the stoichiometry of the precursors. These 2θ values (28.35°–28.55°) and d_{112} (3.121–3.144 Å) align with literature for kesterite CZTS, e.g., 2θ ~28.3° and d ~3.14 Å in sprayed films – as in ultrasonic spray [11]. Crystallite sizes (23–33 nm) match annealed CZTS (22–35 nm) [81]. The kesterite phase is characterized by a tetragonal crystal system, and numerous authors have found that these films exhibited a strong preferential orientation along the (112) crystallographic plane – as in CZTS synthesis [81]. In addition to the dominant (112) peak, the presence of other diffraction peaks corresponding to the (220), (312) planes are claimed to be characteristic of a well-formed kesterite CZTS phase. For instance, Ghediya et al. deposited CZTS films using an ultrasonic spray method. Their XRD results revealed three broad diffraction peaks at 2Θ values of 28.3º, 47.6 º and 56.1 º, corresponding to (112), (220) and (312) planes of tetragonal kesterite CZTS. According to the authors, the absence of peaks associated with secondary sulfides or oxides indicated phase purity within the detection limit of XRD – as in CZTS synthesis [81]. Iliyas et al. reported the synthesis of V-doped CZTS thin films by chemical spray pyrolysis method. According to their XRD patterns, undoped CZTS thin films showed four diffraction peaks corresponding to (112), (200), (220) and (312) planes of kesterite structure of CZTS, revealing that no subsequent binary or ternary phases were present during the formation of the distinctive tetragonal kesterite structure.

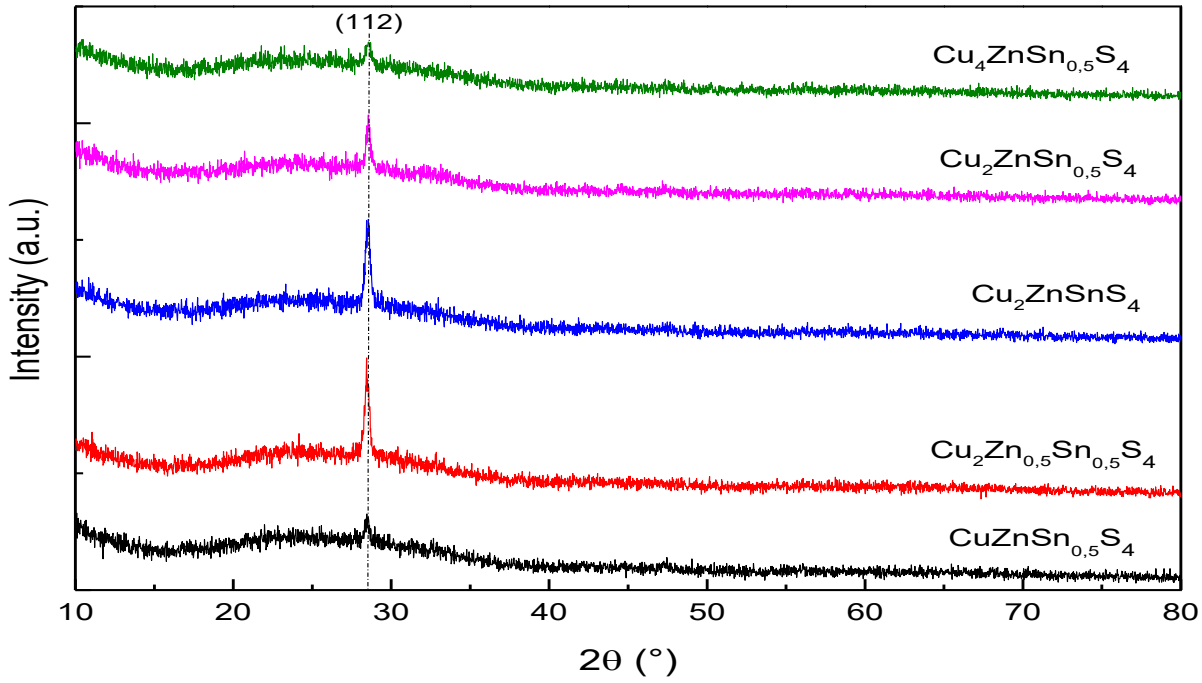


Figure 10 XRD patterns of CZTS thin films with different Cu:Zn:Sn atomic ratios.

### 4.2.2 Morphological Analysis

**Results:** Scanning electron microscopy (SEM) images of samples with (Cu:Zn:Sn:S) atomic ratios of (1:1:0.5:4), (2:0.5:0.5:4), (2:1:1:4), (2:1:0.5:4) and (4:1:0.5:4) at 50,000 magnification are presented in Fig. 3. The films revealed different surface morphologies depending on the stoichiometry state. Generally, the film surface is compact without significant defects such as cracks or voids. Some coarse nodules were mainly observed on the surface of films synthesized with (Cu:Zn:Sn:S) atomic ratios corresponding to (1:1:0.5:4), (2:0.5:0.5:4) and (2:1:0.5:4). A relatively uniform grain distribution was clearly observed for the sample with ideal stoichiometry ($Cu_2ZnSnS_4$). For the copper-rich—tin-deficient (4:1:0.5:4) sample, the grains size became smaller.

**Discussion:** A similar phenomenon of nodules was observed by Moreno-Regino et al. [40] in their CZTS films prepared by spray technique. The authors attributed these nodules to the interaction of sulfur with active sites on the film's surface. Uniform grain distribution in the stoichiometric sample is beneficial in photovoltaic applications as it can reduce recombination of photogenerated carriers [41]. These scanning electron microscopy observations are fully consistent with XRD results – as in CZTS morphology [81]. Fig. 9 shows the surface topography (side-view 3D AFM images) of samples with (Cu:Zn:Sn:S) atomic ratios corresponding to (2:1:1:4), (2:0.5:0.5:4), (2:1:0.5:4), (1:0.5:0.5:4),

(4:1:1:4) deposited onto glass substrates. The films are quite homogeneous and the surface morphology changes according to the (Cu:Zn:Sn:S) atomic ratio. The surface became quite rough for the copper-rich—zinc-deficient (4:1:0.5:4) sample as shown in Fig. 4. The surface is fully homogeneous for the stoichiometric (2:1:1:4) films in agreement with that seen in SEM analysis – as in Sn concentration [11].

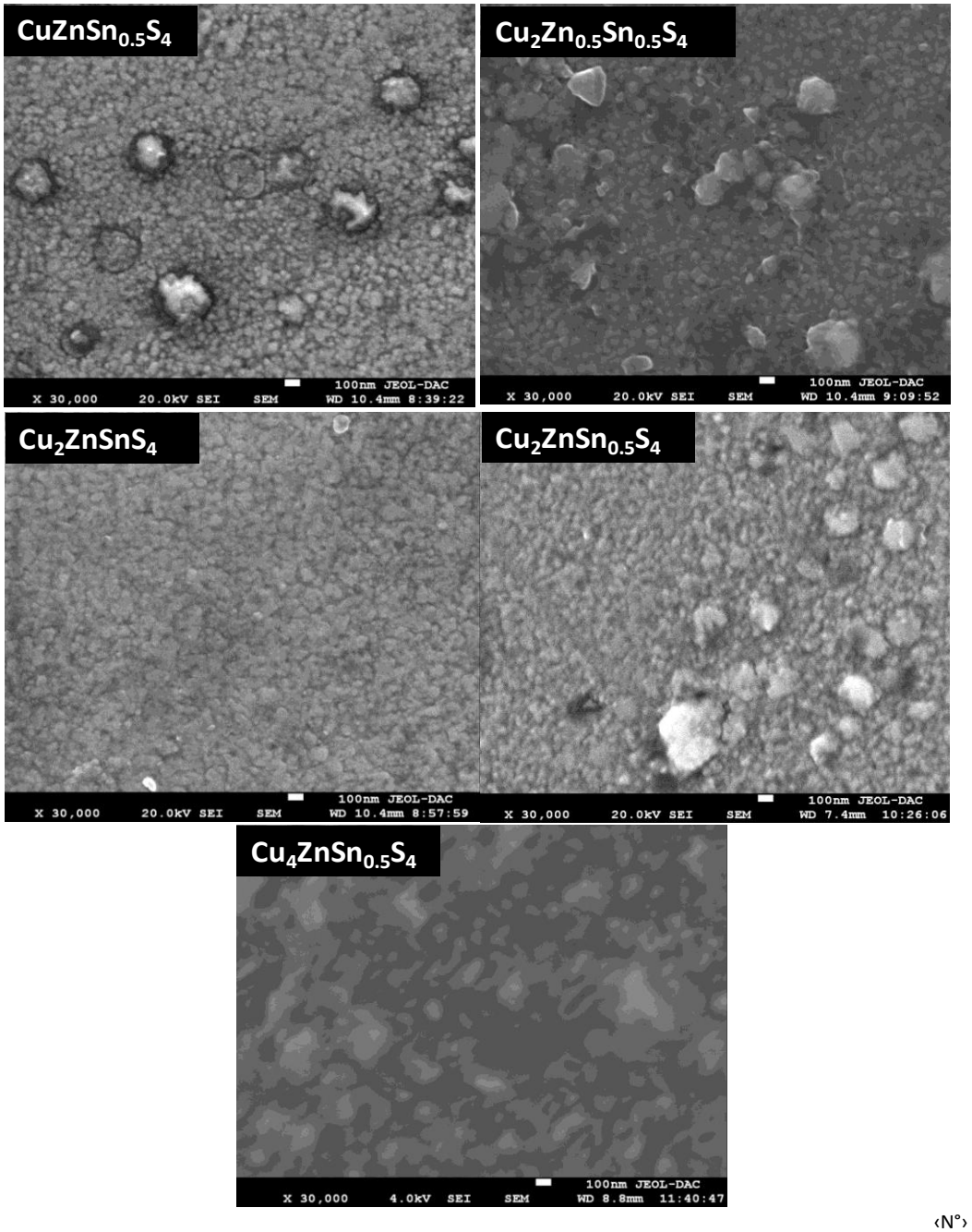


‹N°›

Figure 11 SEM images of CZTS thin films with various Cu:Zn:Sn:S atomic ratios

### 4.2.3 Atomic Force Microscopy (AFM) Analysis

**Results:** The surface morphology of the films was further analyzed using AFM, with the results shown in Fig. 4. The AFM analysis confirmed that the films' roughness and grain size were heavily dependent on the stoichiometry. The (2:1:1:4) sample exhibited the lowest surface roughness. For the zinc and tin-deficient (2:0.5:0.5:4) sample, increased roughness and smaller grains were observed.

**Discussion:** The ideal composition promotes smoother surfaces, which are advantageous for photovoltaic applications [81]. The increased roughness in the zinc and tin-deficient sample could result in higher recombination rates at grain boundaries, thereby reducing device efficiency [81].

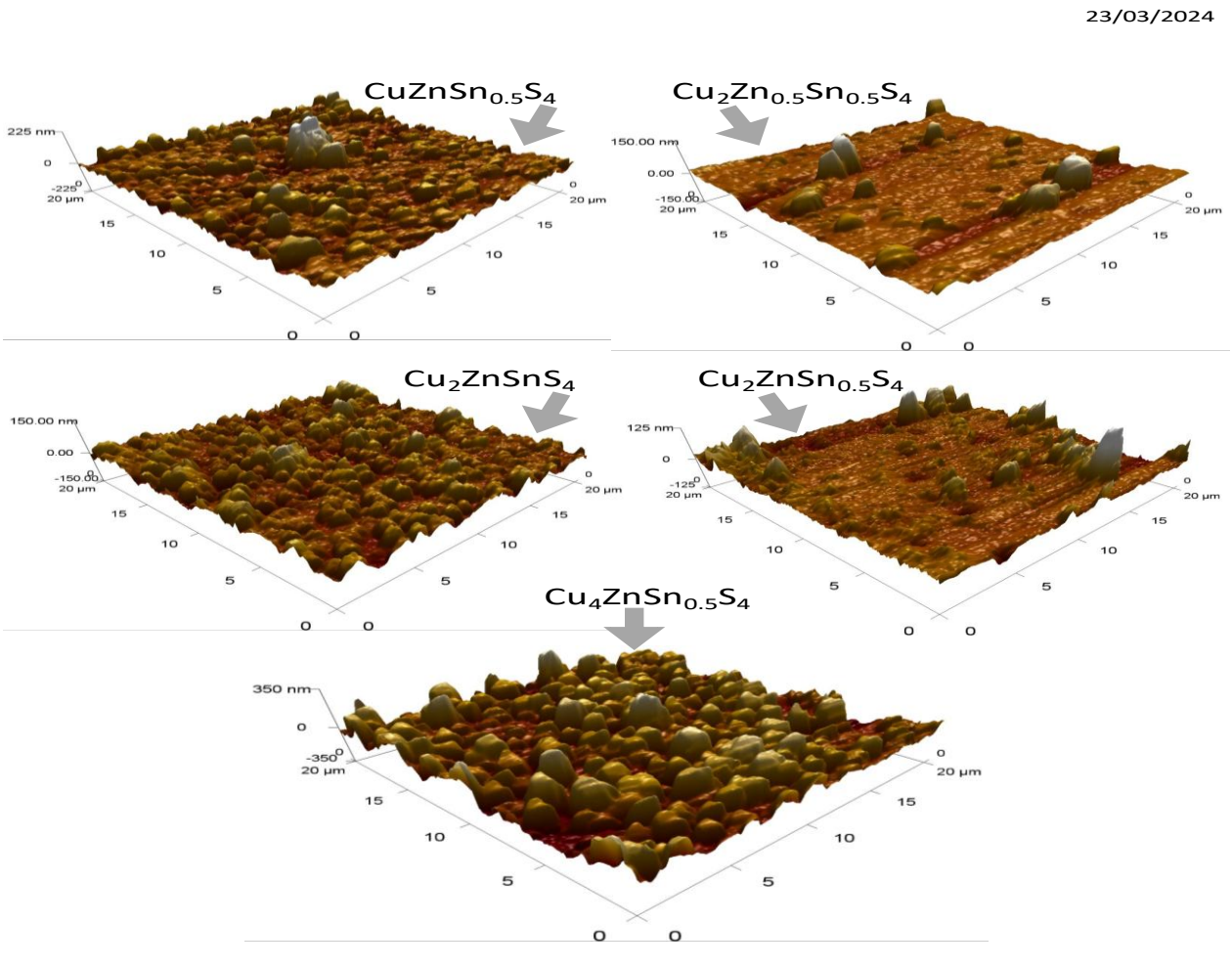


Figure 12 AFM 3D topographical images of CZTS thin films with different Cu:Zn:Sn atomic ratios.

### 4.2.4 Optical Analysis

**Results:** The transmittance curves of the samples with different Cu:Zn:Sn:S atomic ratios are shown in Fig. 14. The spectra revealed significant variations in optical transmission based on the film's composition. The optical band gap (Eg) of the prepared samples was calculated using the Tauc plot, shown in the inset of Fig. 14. The tin-deficient ($Cu_2ZnSn_{0.5}S_4$) film exhibits the widest gap (Eg=1.81 eV), while the zinc-tin-deficient ($Cu_2Zn_{0.5}Sn_{0.5}S_4$) sample exhibits the narrowest band gap (Eg=1.14 eV). The stoichiometric ($Cu_2ZnSnS_4$) film exhibits a value of 1.48 eV. The band gap energy of the copper-tin-deficient ($CuZnSn_{0.5}S_4$) and copper-rich/tin-deficient ($Cu_4ZnSn_{0.5}S_4$) samples was found to be 1.52 eV and 1.28 eV, respectively.

**Discussion:** Our results align with previous studies, including those by Camara et al. [42], which emphasize the importance of Zn content in enhancing transparency. These findings demonstrate the potential to engineer the optical properties of CZTS compounds through compositional modifications, thereby enabling tailored applications in solar cells and other optoelectronic devices – as in Sn concentration [11]. Stoichiometry plays a pivotal role in determining a film's band gap. Specifically, tin-deficient samples exhibit wider band gaps due to alterations in the lattice parameters, which induce lattice strain, and the formation of native point defects that modify the electronic band structure. Conversely, zinc-tin-deficient samples show narrower band gaps, illustrating how varying these elements' proportions can tailor the films' optical properties for specific applications. The observed trends in band gap variations are consistent with those reported by Choi et al. [44]. Additionally, the range of the obtained band gap values is in good agreement with other works on spray-deposited CZTS – as in Ge-alloyed [18]. This change is primarily attributed to two factors: (1) alterations in the lattice parameters, which induce lattice strain, and (2) the formation of a high concentration of native point defects and defect clusters. These defects introduce states near the band edges (a phenomenon known as band tailing), which directly modify the electronic band structure and, consequently, the measured optical band gap – as in defect studies [10]. The ability to engineer the band gap through stoichiometric adjustments provides a clear pathway for optimizing CZTS-based materials for specific photovoltaic and optoelectronic applications. For instance, the lower band gap (1.14 eV) is suitable for devices requiring broader solar spectrum absorption. Conversely, the higher band gap (1.81 eV) is ideal for applications like top cells in tandem devices. For example, Diwate et al. studied CZTS thin films deposited by spray pyrolysis at various substrate temperatures.

Their research highlighted that the optical band gap values varied from 2.0 to 2.25 eV, suggesting that quantum confinement effects at the nanoscale, controlled by thermal conditions, could be another significant factor in band gap variation. These results demonstrate that both compositional engineering, as explored in our work, and the control of process-induced nanostructural features are powerful tools for tuning the optical properties of CZTS [11].

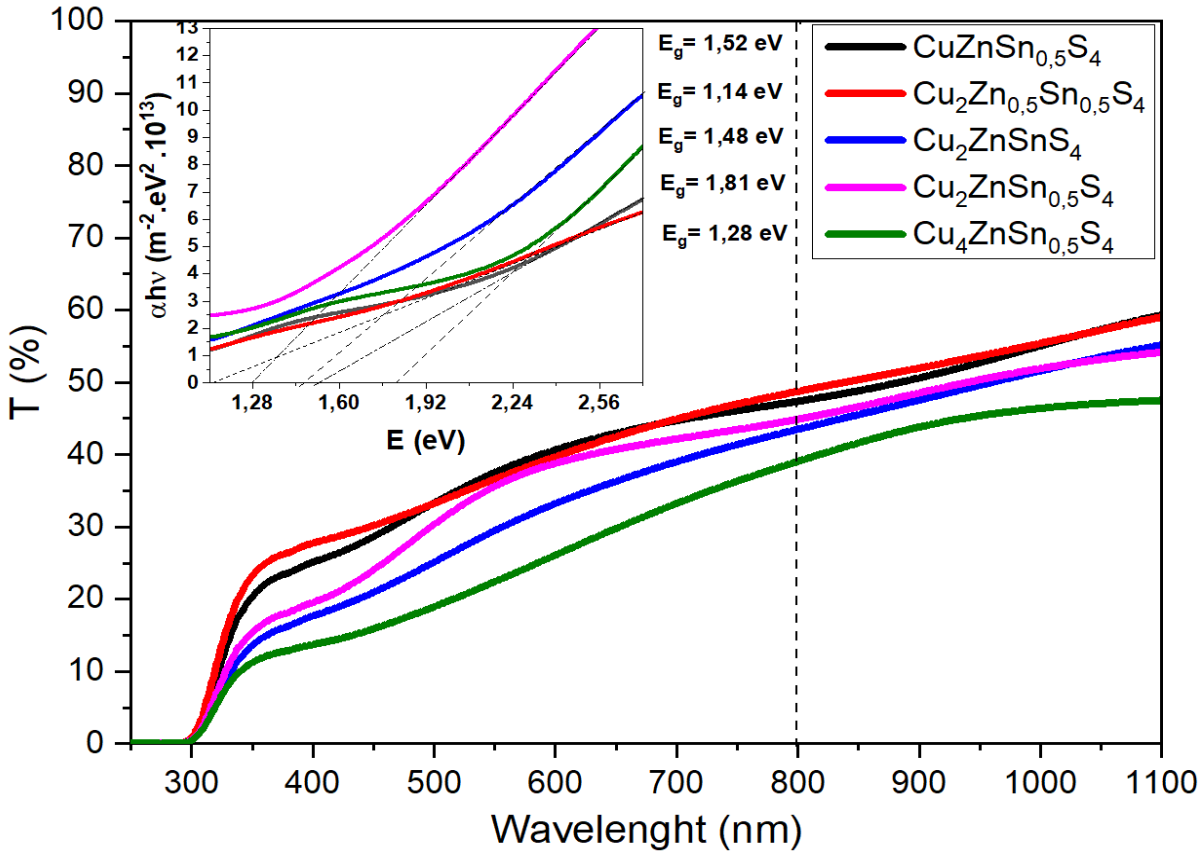


Figure 13 UV-Vis Absorption Spectra of CZTS thin films. Optical Absorption and Bandgap Analysis of CZTS thin films.

### 4.2.5 Electrochemical Investigations

### 4.2.6 Photocurrent Response

**Results:** Fig. 15 shows the photocurrent response for CZTS films deposited at different atomic ratios. Spikes were observed in the curves for all CZTS films. All films exhibited negative photocurrent indicating p-type conductivity. The (2:1:1:4) sample exhibited the highest photocurrent response of 2.54 µA during the "ON" state. The zinc-tin-deficient film exhibits a lower current response, ranging from approximately -0.2 to 0.2 µA, with a peak of 0.91 µA during the "ON" state. For the tin-deficient

film (4:1:0.5:4), a current response ranging from approximately -1.6 to 1.2 μA, peaking at 1.64 μA during the "ON" state was observed.

**Discussion:** Such photoresponse tests evaluate the efficiency and speed of charge carrier generation and recombination in materials, which are critical parameters in PEC applications. Borate et al. [51] reported a similar result when they prepared CZTS film by electrodeposition method. The authors claimed that, when the electrode is illuminated, the generated electrons move towards the electrolyte and the holes migrate towards the back electrode (photocathode), leading to the formation of spikes in the photocurrent curves. The negative photocurrent is due to proton (H+) reduction on the working electrodes [52]. The reduced current response in the zinc-tin-deficient film could be attributed to the lower concentrations of Zn and Sn, thus affecting the conductivity and photoresponse efficiency. The increased Zn content in the tin-deficient film enhanced the material's conductivity, resulting in a higher current response – as in CZTS photocathodes [97].

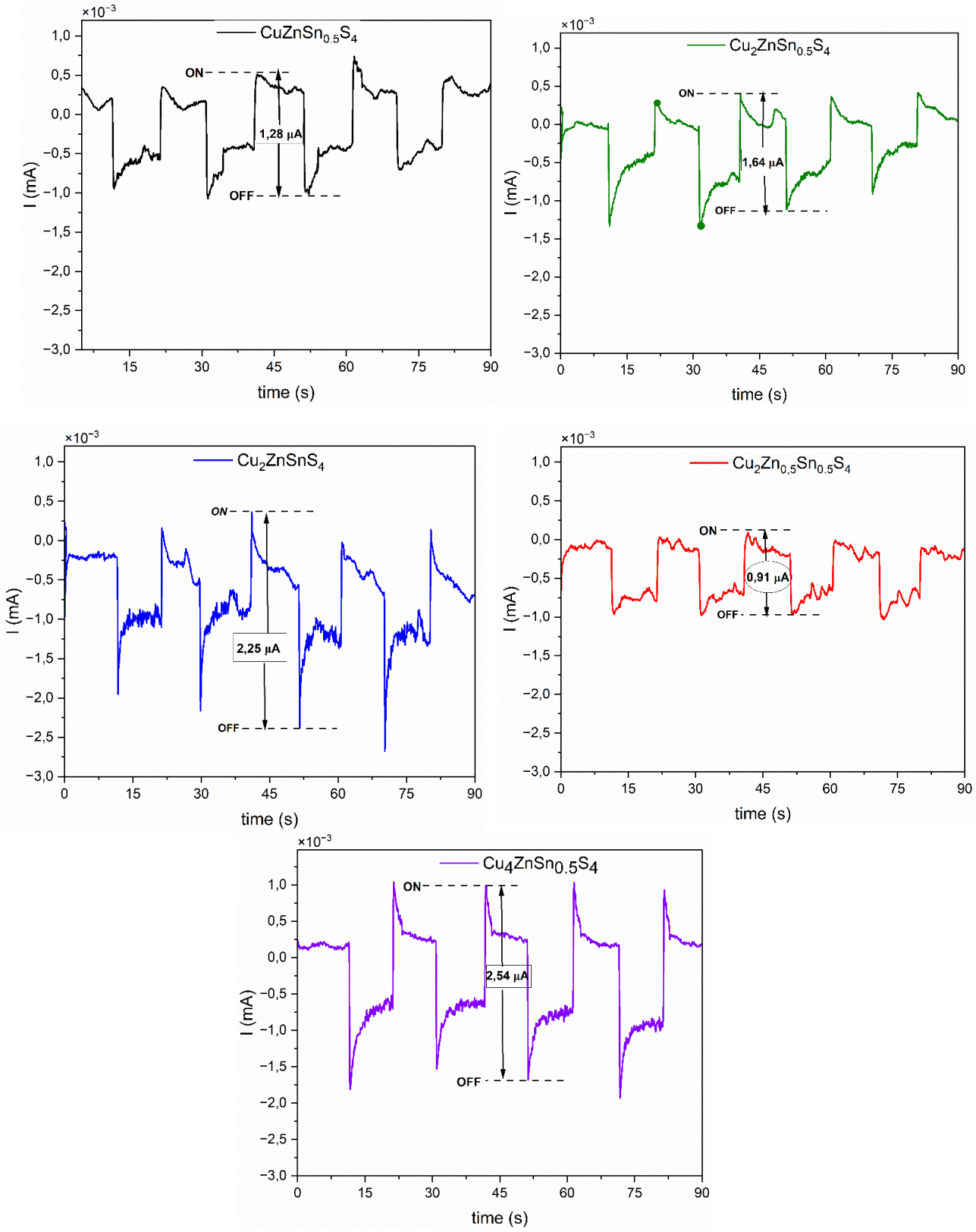


Figure 14 Photocurrent response of CZTS thin films under UV illumination.

### 4.2.7 Current Density-Voltage (J-V) Characteristics

**Results:** Fig. 16 presents the linear sweep voltammetry (LSV) curves of CZTS photocathodes for the zinc-tin-deficient (2:0.5:0.5:4) and stoichiometric (2:1:1:4) film. The photocathode exhibited improved photocurrent density upon illumination. The current density increases more significantly under illumination for $Cu_2ZnSnS_4$ films compared to the zinc-tin-deficient (2:0.5:0.5:4) film. The current density reaches around -10.57 mA/cm² at approximately -1.02 V (vs. Ag/AgCl).

**Discussion:** A similar electrochemical photocurrent trend was obtained by Mahalakshmi et al. [53]. The authors studied the effect of annealing time on the photoelectrochemical properties of CZTS nanoparticles synthesized by a simple one-step chemical method using a non-toxic solvent (water) and found a similar photocurrent trend, which is the expected behavior for p-type semiconductors. Mali et al. [54] deposited CZTS thin films on fluorine-doped tin oxide/glass (glass/FTO) substrates using the successive ionic layer adsorption and reaction (SILAR) method. The authors obtained similar trend in their current density–voltage (J–V) curves under dark and illumination conditions – as in CZTS PEC [99].

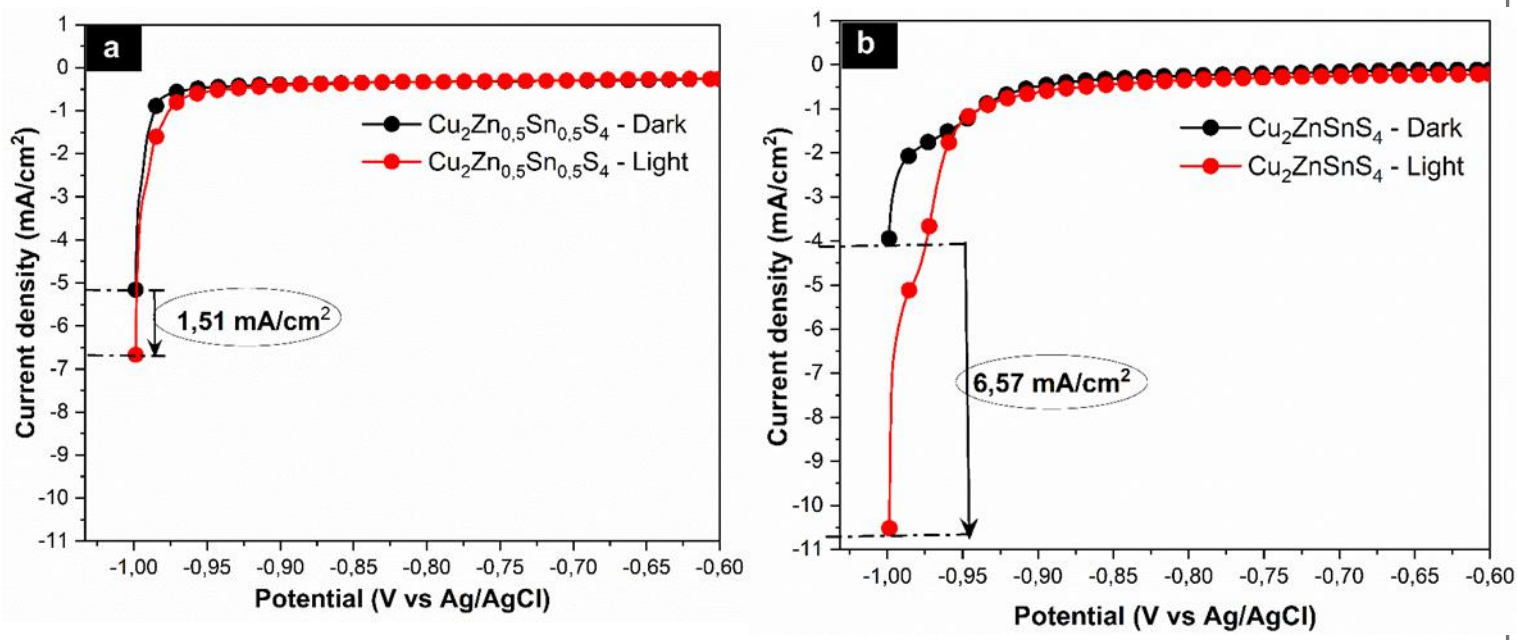


.

Figure 15 J-V characteristics of CZTS thin films under dark and illuminated conditions.

### Conclusion

This chapter presented a detailed analysis of the structural, morphological, optical, and electrochemical properties of CZTS thin films with varying Cu:Zn:Sn atomic ratios. The findings emphasize the importance of compositional control in optimizing the material's performance for photovoltaic applications. The ideal stoichiometric ratio (2:1:1:4) was found to produce the highest quality films, with superior crystallinity, surface morphology, and photocurrent response. These results provide a solid foundation for further optimization of CZTS thin films and contribute to the ongoing development of cost-effective, high-efficiency solar cells.

### Final Remarks

This thesis has demonstrated that pure $Cu_2ZnSnS_4$ thin films can be deposited via a multi-spray process. The four elements of interest were mixed in the vapor state, unlike previous spray configurations. The setup was optimized to precisely tune the atomic ratio of the source materials and achieve a kesterite CZTS single-phase with promising performance in PEC applications. X-ray diffraction (XRD) analysis indicated that phase formation was strongly dependent on the Cu:Zn:Sn:S atomic ratios. In all cases, pure $Cu_2ZnSnS_4$ kesterite phase structure with (112) orientation was obtained. Notably, stoichiometric films exhibited excellent structural, morphological and electrochemical properties, with photocurrent densities reaching up to 6 $mA/cm^2$. Thus, this approach offers a potential route to prepare uniform films using low-cost precursors and materials, without requiring sulfurization or selenization process. The prepared films (photocathodes) are useful in PEC water splitting applications – as in high-STH CZTS [96]

# 5 General Conclusion

This thesis has successfully introduced and optimized an innovative multi-spray pyrolysis method for the fabrication of high-quality $Cu_2ZnSnS_4$ (CZTS) thin films. By employing independent atomization of the four precursors ($Cu^{2+}$, $Zn^{2+}$, $Sn^{2+}$, and $S^{2-}$) followed by controlled mixing in the vapor phase within a central collector tube, the developed technique effectively overcomes the primary limitations of conventional single-solution spray pyrolysis, including premature chemical reactions, poor stoichiometric control, and the necessity of toxic sulfurization post-treatments.

Under the optimized conditions (Cu:Zn:Sn:S atomic ratio of 2:1:1:4 and substrate temperature of 390 °C), the process yielded single-phase kesterite CZTS films with a strong preferential (112) orientation, crystallite sizes up to 33 nm, and the absence of detectable secondary phases within the resolution limits of XRD. Morphological characterization revealed compact, uniform grains with significantly reduced surface roughness, while optical measurements confirmed an ideal bandgap of 1.48 eV and strong visible-light absorption. Photoelectrochemical investigations demonstrated superior performance, with the stoichiometric films exhibiting the highest photocurrent response (2.54 μA) and the lowest charge-transfer resistance under illumination, confirming efficient p-type conductivity and charge separation.

The practical significance of this work lies in establishing a low-cost, scalable, and environmentally benign route to earth-abundant CZTS thin films suitable for thin-film solar cells and photoelectrochemical water splitting for green hydrogen production. By eliminating hazardous sulfurization steps and achieving precise stoichiometric control, the multi-spray approach represents a meaningful advancement toward sustainable renewable energy technologies.

While XRD, SEM, AFM, UV-Vis, and EIS analyses collectively support the high quality of the deposited films, the study acknowledges the limitation of not having access to complementary techniques such as Raman spectroscopy or XPS for definitive secondary-phase identification. Future research will therefore focus on implementing these analyses, evaluating long-term operational stability, integrating the optimized films on flexible substrates, and exploring tandem cell configurations.

In conclusion, this thesis establishes a novel and effective multi-spray pyrolysis strategy that delivers pure kesterite CZTS thin films with promising photoelectrochemical properties. The findings open new pathways for the development of cost-effective, non-toxic photovoltaic and hydrogen-generation devices, contributing to the global transition toward sustainable energy solutions.

# *REFERENCES*

## REFERENCES


[1] L. He, S. Zhang, Y. Chen, L. Ren, and J. Li, "Techno-economic potential of a renewable energy-based microgrid system for a sustainable large-scale residential community in Beijing, China," *Renewable and Sustainable Energy Reviews*, vol. 93, pp. 631–641, 2018, doi: 10.1016/j.rser.2018.05.053.

[2] X. Li, P. Li, Z. Wu, D. Luo, H. Y. Yu, and Z. H. Lu, "Review and perspective of materials for flexible solar cells," *Materials Reports: Energy*, vol. 1, no. 1, p. 100001, Feb. 2021, doi: 10.1016/J.MATRE.2020.09.001.

[3] S. W. Choi *et al.*, "Flexible and transparent thin-film light-scattering photovoltaics about fabrication and optimization for bifacial operation," *npj Flexible Electronics 2023 7:1*, vol. 7, no. 1, pp. 1–10, Mar. 2023, doi: 10.1038/s41528-023-00251-6.

[4] F. Yang, J. C. Meerman, and A. P. C. Faaij, "Carbon capture and biomass in industry: A techno-economic analysis and comparison of negative emission options," *Renewable and Sustainable Energy Reviews*, vol. 144, p. 111028, 2021, doi: 10.1016/j.rser.2021.111028.

[5] S. Ullah, A. Bouich, H. Ullah, B. Mari, and M. Mollar, "Comparative study of binary cadmium sulfide (CdS) and tin disulfide (SnS2) thin buffer layers," *Solar Energy*, vol. 208, pp. 637–642, 2020, doi: 10.1016/j.solener.2020.08.036.

[6] K. Jin and X. Liu, "Chemical activity, oxidation resistance and infrared transparency of (Ti3C2)n quantum dots induced by quantum confinement effect," *Surfaces and Interfaces*, vol. 44, p. 103790, 2024, doi: 10.1016/j.surfin.2023.103790.

[7] R. S. Sundari *et al.*, "Effective decoupling of grain boundaries and secondary phase interfaces for enhanced thermoelectric performance of Cu1.8S/WS2 nanocomposites," *J. Alloys Compd.*, vol. 960, p. 170796, 2023, doi: 10.1016/j.jallcom.2023.170796.

[8] R. Massadeh and M. M. Hamasha, "Comprehensive review of CZTS deposition techniques and experimental insights into low-temperature chemical synthesis of CZTS thin film solar cells," *Opt. Mater. (Amst).*, vol. 157, p. 116427, 2024, doi: 10.1016/j.optmat.2024.116427.

[9] M. J. Romero, H. Du, G. Teeter, Y. Yan, and M. M. Al-Jassim, "Comparative study of the luminescence and intrinsic point defects in the kesterite Cu2ZnSnS4and chalcopyrite Cu(In,Ga)Se2thin films used in photovoltaic applications," *Phys. Rev. B*, vol. 84, no. 16, 2011, doi: 10.1103/physrevb.84.165324.

[10] M. Sultana *et al.*, "Fabrication of $Cu_2ZnSnS_4$ (CZTS) thin films by ultrasonic spray pyrolysis at a low substrate temperature and effect of tin concentration on the characteristics of the CZTS thin films," *Bangladesh Journal of Scientific and Industrial Research*, vol. 57, no. 1, pp. 1–6, 2022, doi: 10.3329/bjsir.v57i1.58894.

[11] K. Jeganath and R. Y, "Near-optimal composition of CZTS thin film via exploration of copper and thiourea molar concentration in spray pyrolysis technique," *Mater. Res. Express*, vol. 8, no. 11, p. 116404, 2021, doi: 10.1088/2053-1591/ac343e.

[12] T. H. Nguyen *et al.*, "Structural and Solar Cell Properties of a Ag-Containing $Cu_2ZnSnS_4$Thin Film Derived from Spray Pyrolysis," *ACS Appl. Mater. Interfaces*, vol. 10, no. 6, pp. 5455–5463, 2018, doi: 10.1021/acsami.7b14929.

[13] M. F. Islam, N. M. Yatim, and M. A. Hashim@Ismail, "A Review of CZTS Thin Film Solar Cell Technology," *Journal of Advanced Research in Fluid Mechanics and Thermal Sciences*, vol. 81, no. 1, pp. 73–87, 2021, doi: 10.37934/arfmts.81.1.7387.

[14] M. Khushaim, S. Alamri, N. Kattan, A. Jaber, and S. Alamri, "Study of kesterite $Cu_2ZnSnS_4$ (CZTS) thin films deposited by spray technique for

photovoltaic applications," *Journal of Taibah University for Science*, vol. 15, no. 1, pp. 329–339, 2021, doi: 10.1080/16583655.2021.1978809.

[15] A. A. Zgliui, M. S. Tivanov, N. N. Curmei, L. V. Dermenji, L. I. Bruc, and D. A. Serban, "Structure of Ag-Containing Cu2ZnSnS4 Thin Films, Obtained by Spray Pyrolysis," *Applied Solar Energy (English translation of Geliotekhnika)*, vol. 59, no. 3, pp. 189–200, Jun. 2023, doi: 10.3103/S0003701X23600790/METRICS.

[16] S. T. Yussuf *et al.*, "Novel heterojunction superstrate Cu2ZnInS4−x (CZIS) thin film kesterite solar cell with vertical arrays of hexagonal ZnO nanorods window layer," *J. Alloys Compd.*, vol. 935, p. 168211, Feb. 2023, doi: 10.1016/J.JALLCOM.2022.168211.

[17] D. B. Khadka, S. Kim, and J. Kim, "Ge-alloyed CZTSe thin film solar cell using molecular precursor adopting spray pyrolysis approach," *RSC Adv.*, vol. 6, no. 44, pp. 37621–37627, 2016, doi: 10.1039/c6ra02291j.

[18] W. Cui *et al.*, "Preparation of CZTS film by electro-deposition method: study on the principle of deposition and film performance," *Journal of Materials Science: Materials in Electronics*, vol. 32, no. 20, pp. 25188–25200, Oct. 2021, doi: 10.1007/S10854-021-06975-3/METRICS.

[19] M. Oubakalla *et al.*, "Effects of copper concentration on the properties of Cu2CoSnS4 thin films co-electrodeposited on the FTO substrate," *Journal of Materials Science: Materials in Electronics*, vol. 33, no. 15, pp. 12016–12025, May 2022, doi: 10.1007/S10854-022-08162-4/METRICS.

[20] W. Menadi *et al.*, "Correlation between physical properties and growth mechanism of ultrasonic-sprayed Cu2ZnSnS4 based thin films with different solution flow rates," *Physica B Condens. Matter*, p. 416944, Jan. 2025, doi: 10.1016/J.PHYSB.2025.416944.

[21] A. Hammoud *et al.*, "Spray Pyrolysis Technique for $Cu_2MgSnS_4$ Thin Films," *Thin Films - Fundamentals, Deposition Techniques and Applications [Working Title]*, Mar. 2025, doi: 10.5772/INTECHOPEN.1009567.

[22] A. K. Singh, T. R. Rana, J. Kim, M. Shkir, and T. C. Jen, "Impact on Structural and Optical Properties of CZTS Thin Films with Solvents and Ge Incorporation," *International Journal of Photoenergy*, vol. 2021, no. 1, p. 1508469, Jan. 2021, doi: 10.1155/2021/1508469.

[23] D. Huang and C. Persson, "Band gap change induced by defect complexes in Cu2ZnSnS 4," *Thin Solid Films*, vol. 535, no. 1, pp. 265–269, 2013, doi: 10.1016/j.tsf.2012.10.030.

[24] S. Das, K. J. Zavalla, M. A. Mannan, and K. C. Mandal, "Fabrication and characterization of low-cost, Large-area spray deposited Cu2ZnSnS4 thin films for heterojunction solar cells," *Materials Research Society Symposium Proceedings*, vol. 1538, no. 1, pp. 115–121, Dec. 2013, doi: 10.1557/OPL.2013.1001/METRICS.

[25] J. Bisquert, F. Fabregat-Santiago, I. Mora-Seró, G. Garcia-Belmonte, E. M. Barea, and E. Palomares, "A review of recent results on electrochemical determination of the density of electronic states of nanostructured metal-oxide semiconductors and organic hole conductors," *Inorganica Chim. Acta*, vol. 361, no. 3, pp. 684–698, Feb. 2008, doi: 10.1016/J.ICA.2007.05.032.

[26] A. Abdel-Galil and N. L. Moussa, "Deposition of nano-crystalline Cu2ZnSnS4 thin film in one step without sulfurization: Future prospects," *J. Mater. Res.*, vol. 39, no. 7, pp. 1139–1153, Apr. 2024, doi: 10.1557/S43578-024-01298-5/FIGURES/8.

[27] Amrut Agasti and Parag Bhargava, "Phase Evolution during Ageing of Co-Electrodeposited Cu–Zn–Sn Thin Films and Effect of Soft Annealing," *Applied Solar Energy (English translation of Geliotekhnika)*, vol. 60, no. 1, pp. 1–8, Feb. 2024, doi: 10.3103/S0003701X23601382/METRICS.

[28] R. Rajasekar, M. SenthilKumar, S. Shanmugan, and M. Nagarajan, "The influence of Cu2ZnSnS4 thin films with characteristics of treatment conditions on spray pyrolysis technique for solar cells applications," *Indian Journal of Physics*, vol. 96, no. 3, pp. 707–716, Mar. 2022, doi: 10.1007/S12648-020-01999-7/METRICS.

[29] T. H. Nguyen, W. Septina, S. Fujikawa, F. Jiang, T. Harada, and S. Ikeda, "$Cu_2ZnSnS_4$thin film solar cells with 5.8% conversion efficiency obtained by a facile spray pyrolysis technique," *RSC Adv.*, vol. 5, no. 95, pp. 77565–77571, 2015, doi: 10.1039/c5ra13000j.

[30] S. Thiruvenkadam *et al.*, "Effect of Zn/Sn molar ratio on the microstructural and optical properties of Cu 2 Zn 1-x Sn x S 4 thin films prepared by spray pyrolysis technique," *Physica B Condens. Matter*, vol. 533, pp. 22–27, 2018, doi: 10.1016/j.physb.2017.12.065.

[31] S. Mahjoubi, N. Bitri, H. Bouzouita, M. Abaab, and I. Ly, "Effect of the annealing and the spraying time on the properties of CZTS thin films prepared by the 'Spray sandwich' technique," *Applied Physics A*, vol. 123, no. 6, 2017, doi: 10.1007/s00339-017-1020-4.

[32] M. Kumar, A. Dubey, N. Adhikari, S. Venkatesan, and Q. Qiao, "Strategic review of secondary phases, defects and defect-complexes in kesterite CZTS-Se solar cells," *Energy Environ. Sci.*, vol. 8, no. 11, pp. 3134–3159, Nov. 2015, doi: 10.1039/C5EE02153G.

[33] J. P. Sawant and R. B. Kale, "Study on Spray-Deposited Cu2ZnSnS4 Thin Films: Deposition and Physical Properties," pp. 115–124, 2020, doi: 10.1007/978-981-15-2666-4_12.

[34] R. K. Singh, A. Kumar, N. Jain, J. Singh, R. K. Singh, and R. Kumar, "Solution Processed Hybrid Organic-Inorganic CH3NH3PbI3 Perovskite Material and Optical Properties," *Mater. Today Proc.*, vol. 4, no. 14, pp. 12661–12665, 2017, doi: 10.1016/j.matpr.2017.10.079.

[35] D. G. Ovalle, A. Pezo, and A. Manchon, "Influence of the surface states on the nonlinear Hall effect in Weyl semimetals," 2022, *arXiv*. doi: 10.48550/ARXIV.2206.08681.

[36] A. A. Ahmad, A. B. Migdadi, A. M. Alsaad, I. A. Qattan, Q. M. Al-Bataineh, and A. Telfah, "Computational and experimental characterizations of annealed Cu2ZnSnS4 thin films," *Heliyon*, vol. 8, no. 1, p. e08683, 2022, doi: 10.1016/j.heliyon.2021.e08683.

[37] M. Al-Shakban *et al.*, "The synthesis and characterization of Cu2ZnSnS4 thin films from melt reactions using xanthate precursors," *J. Mater. Sci.*, vol. 52, no. 21, pp. 12761–12771, 2017, doi: 10.1007/s10853-017-1367-0.

[38] D. of E. L.I.S Laboratory Faculty of Technology University of Setif 1 19000 Setif Algeria, M. Abderrezek, M. Fathi, D. of E. L.I.S Laboratory Faculty of Technology University of Setif 1 19000 Setif Algeria, F. Djahli, and D. of E. L.I.S Laboratory Faculty of Technology University of Setif 1 19000 Setif Algeria, "Comparative Study of Temperature Effect on Thin Film Solar Cells," *Journal of Nano- and Electronic Physics*, vol. 10, no. 2, pp. 02027-1-02027–6, 2018, doi: 10.21272/jnep.10(2).02027.

[39] H. Deng *et al.*, "Novel symmetrical bifacial flexible CZTSSe thin film solar cells for indoor photovoltaic applications," *Nat. Commun.*, vol. 12, no. 1, 2021, doi: 10.1038/s41467-021-23343-1.

[40] A. Ganai, P. S. Maiti, L. Houben, R. Bar-Ziv, and M. Bar Sadan, "Inside-Out: The Role of Buried Interfaces in Hybrid $Cu_2ZnSnS_4$–Noble Metal Photocatalysts," *The Journal of Physical Chemistry C*, vol. 121, no. 12, pp. 7062–7068, 2017, doi: 10.1021/acs.jpcc.7b01733.

[41] A. Yaghoubi and X. Hao, "Polymorphs of Copper Zinc Tin Sulfide: Optoelectronic Properties and Detection Using Raman," *Solar RRL*, vol. 8, no. 9, p. 2400010, May 2024, doi: 10.1002/SOLR.202400010.

[42] S. Y. Gezgin, W. Belaid, M. A. B.-M. Kabatas, Y. R. Eker, and H. Ş. Kilic, "Microstrain effects of laser-ablated Au nanoparticles in enhancing CZTS-based 1 Sun photodetector

devices," *Physical Chemistry Chemical Physics*, vol. 26, no. 12, pp. 9534–9545, 2024, doi: 10.1039/d4cp00238e.

[43] D. Bhale *et al.*, "Study of optical and structural properties of CZTS thin films using copper capping layer and sulfurization to correct stoichiometry," *Phys. Scr.*, vol. 99, no. 3, p. 035903, Feb. 2024, doi: 10.1088/1402-4896/AD2048.

[44] T. Shibuya *et al.*, "From kesterite to stannite photovoltaics: Stability and band gaps of the Cu2(Zn,Fe)SnS4 alloy," *Appl. Phys. Lett.*, vol. 104, no. 2, p. 21912, Jan. 2014, doi: 10.1063/1.4862030/132361.

[45] J. M. Skelton, A. J. Jackson, M. Dimitrievska, S. K. Wallace, and A. Walsh, "Vibrational spectra and lattice thermal conductivity of kesterite-structured Cu2ZnSnS4 and Cu2ZnSnSe4," *APL Mater.*, vol. 3, no. 4, p. 041102, 2015, doi: 10.1063/1.4917044.

[46] Y. Yang, Y. Ding, J. Zhang, N. Liang, L. Long, and J. Liu, "Insight into the Growth Mechanism of Mixed Phase CZTS and the Photocatalytic Performance," *Nanomaterials*, vol. 12, no. 9, p. 1439, 2022, doi: 10.3390/nano12091439.

[47] C. Platzer Björkman, J. K. Larsen, N. Saini, M. Babucci, and N. Martin, "Ultrathin wide band gap kesterites," *Faraday Discuss.*, vol. 239, pp. 38–50, 2022, doi: 10.1039/D2FD00052K.

[48] B. Monserrat, J.-S. Park, S. Kim, and A. Walsh, "Role of electron-phonon coupling and thermal expansion on band gaps, carrier mobility, and interfacial offsets in kesterite thin-film solar cells," 2018, doi: 10.48550/ARXIV.1805.00022.

[49] S. M. Kobosko, J. T. DuBose, and P. V Kamat, "Perovskite Photocatalysis. Methyl Viologen Induces Unusually Long-Lived Charge Carrier Separation in $CsPbBr_3$ Nanocrystals," *ACS Energy Lett.*, vol. 5, no. 1, pp. 221–223, 2020, doi: 10.1021/acsenergylett.9b02573.

[50] K. Yin *et al.*, "Gradient bandgap enables >13% efficiency sulfide Kesterite solar cells with open-circuit voltage over 800 mV," 2024, *arXiv*. doi: 10.48550/ARXIV.2404.00291.

[51] N. Kata, D. Diouf, A. Darga, and A. Seidou Maiga, "The effect of the recombination mechanisms location on the temperature sensitivity of thin-film photovoltaic cells," *EPJ Photovoltaics*, vol. 10, p. 8, 2019, doi: 10.1051/epjpv/2019008.

[52] C.-J. Tong *et al.*, "Density Functional Theory and Experimental Determination of Band Gaps and Lattice Parameters in Kesterite $Cu_2 ZnSn(S_x Se_{1-x})_4$," *J. Phys. Chem. Lett.*, vol. 11, no. 24, pp. 10463–10468, 2020, doi: 10.1021/acs.jpclett.0c03205.

[53] M. Koubaa, R. Karray, N. Dhifallah, A. Kabadou, and L. Bsais, "Effect of manganese doping on vibrational and physical properties of ZrTe 3 O 8," *J. Alloys Compd.*, vol. 709, pp. 808–818, 2017, doi: 10.1016/j.jallcom.2017.03.053.

[54] F. Z. Boutebakh, N. Attaf, and M. S. Aida, "Effect of growth temperature on the physical properties of kesterite Cu2ZnSnS4 (CZTS) thin films," *Discov. Mater.*, vol. 5, no. 1, pp. 1–10, Dec. 2025, doi: 10.1007/S43939-025-00179-W/METRICS.

[55] G. Rajesh *et al.*, "Dual-functionality of CZTS nanoflakes: as an anode material for lithium-ion batteries and as a counter electrode in DSSCs – a DFT and experimental investigation," *Energy Advances*, vol. 3, no. 7, pp. 1717–1725, Jul. 2024, doi: 10.1039/D4YA00135D.

[56] J. Xu, X. Tian, and L. Qiu, "Investigation of the properties of CZTS/FTO interface," *Opt. Mater. (Amst).*, vol. 115, no. December 2020, p. 111034, 2021, doi: 10.1016/j.optmat.2021.111034.

[57] M. Guc *et al.*, "Polarized Raman scattering study of kesterite type Cu2ZnSnS4 single crystals," *Sci. Rep.*, vol. 6, no. 1, p. 19414, 2016, doi: 10.1038/srep19414.

[58] K. Hönes, E. Zscherpel, J. Scragg, and S. Siebentritt, "Shallow defects in Cu2ZnSnS4," *Physica B Condens. Matter*, vol. 404, no. 23–24, pp. 4949–4952, 2009, doi: 10.1016/j.physb.2009.08.206.

[59] F. P. M. Kreuwel, W. H. Knap, L. R. Visser, W. G. J. H. M. Van Sark, J. Vilà-Guerau De Arellano, and C. C. Van Heerwaarden, "Analysis of high frequency photovoltaic solar energy fluctuations," *Solar Energy*, vol. 206, pp. 381–389, 2020, doi: 10.1016/j.solener.2020.05.093.

[60] M. Khammar, F. Ynineb, S. Guitouni, Y. Bouznit, and N. Attaf, "Crystallite size and intrinsic strain contribution in band gap energy redshift of ultrasonic-sprayed kesterite CZTS nanostructured thin films," *Applied Physics A*, vol. 126, no. 6, p. 398, 2020, doi: 10.1007/s00339-020-03591-6.

[61] H. S. Nugroho *et al.*, "A progress review on the modification of CZTS(e)-based thin-film solar cells," *Journal of Industrial and Engineering Chemistry*, vol. 105, no. xxxx, pp. 83–110, 2022, doi: 10.1016/j.jiec.2021.09.010.

[62] J. P. Sawant, H. M. Pathan, and R. B. Kale, "Photoelectrochemical Properties of Spray Deposited Cu2ZnSnS4 Photoelectrode: Enhancement in Photoconversion Efficiency with Film Thickness," *ES Energy and Environment*, vol. 10, pp. 73–79, Dec. 2020, doi: 10.30919/ESEE8C933.

[63] Z. Chen, M. Li, Y. Cui, and Y. Wang, "AgVO3/Ag6Si2O7 nanocomposites with enhancing visible-light driven photocatalysis performance," *Materials Today Sustainability*, vol. 24, p. 100591, 2023, doi: 10.1016/j.mtsust.2023.100591.

[64] S. P. Ramkumar, H. P. C. Miranda, X. Gonze, and G.-M. Rignanese, "CZTS Raman spectra beyond kesterite: a first-principles study," 2021, *arXiv*. doi: 10.48550/ARXIV.2101.04472.

[65] H. Zhang *et al.*, "Efficiency enhancement of CZTS solar cell with WO3 buffer layer using CZTSe BSF layer," *Energy Reports*, vol. 12, pp. 2707–2719, Dec. 2024, doi: 10.1016/J.EGYR.2024.08.045.

[66] W. D. Thompson, A. Nandur, and B. E. White, "Thermal transport in Cu2ZnSnS4 thin films," *J. Appl. Phys.*, vol. 119, no. 9, p. 095108, 2016, doi: 10.1063/1.4942661.

[67] M. Minbashi, A. Ghobadi, E. Yazdani, A. A. Kordbacheh, and A. Hajjiah, "Efficiency enhancement of CZTSSe solar cells via screening the absorber layer by examining of different possible defects," *Sci. Rep.*, vol. 10, no. 1, pp. 1–14, Dec. 2020, doi: 10.1038/S41598-020-75686-2.

[68] W. C. Liu, B. L. Guo, X. S. Wu, F. M. Zhang, C. L. Mak, and K. H. Wong, "Facile hydrothermal synthesis of hydrotropic Cu2ZnSnS 4 nanocrystal quantum dots: Band-gap engineering and phonon confinement effect," *J. Mater. Chem. A Mater.*, vol. 1, no. 9, pp. 3182–3186, 2013, doi: 10.1039/c3ta00357d.

[69] S. Lie *et al.*, "Improving Carrier-Transport Properties of CZTS by Mg Incorporation with Spray Pyrolysis," *ACS Appl. Mater. Interfaces*, vol. 11, no. 29, pp. 25824–25832, 2019, doi: 10.1021/acsami.9b05244.

[70] Sadanand, P. K. Singh, S. Rai, P. Lohia, and D. K. Dwivedi, "Comparative study of the CZTS, CuSbS2 and CuSbSe2 solar photovoltaic cell with an earth-abundant non-toxic buffer layer," *Solar Energy*, vol. 222, no. December 2020, pp. 175–185, 2021, doi: 10.1016/j.solener.2021.05.013.

[71] A. I. Inamdar *et al.*, "Optimized fabrication of sputter deposited Cu2ZnSnS4 (CZTS) thin films," *Solar Energy*, vol. 91, pp. 196–203, 2013, doi: 10.1016/j.solener.2013.02.003.

[72] P. K. Singh and U. Kulshrestha, "Unlocking the solar potential: elevating open circuit voltage in kesterite CZTS thin film solar cells through cutting-edge SCAPS modeling,"

*Engineering Research Express*, vol. 7, no. 1, p. 015301, 2025, doi: 10.1088/2631-8695/ada33f.

[73] V. Mahalakshmi, D. Venugopal, K. Ramachandran, and R. Ramesh, "Synthesis of 2D-CZTS nanoplate as photocathode material for efficient PEC water splitting," *Journal of Materials Science: Materials in Electronics*, vol. 33, no. 11, pp. 8493–8503, Apr. 2022, doi: 10.1007/S10854-021-06400-9/METRICS.

[74] X. Xu *et al.*, "Controlling Selenization Equilibrium Enables High-Quality Kesterite Absorbers for Efficient Solar Cells," *Nature Communications 2023 14:1*, vol. 14, no. 1, pp. 1–9, Oct. 2023, doi: 10.1038/s41467-023-42460-7.

[75] J. Chen *et al.*, "Element Diffusion Induced Carrier Transport Enhancement in High-Performance CZTSSe Self-Powered Photodetector," *Small*, vol. 20, no. 24, p. 2307347, Jun. 2024, doi: 10.1002/SMLL.202307347;SUBPAGE:STRING:ABSTRACT;WEBSITE:WEBSITE:PERICLES;REQUESTEDJOURNAL:JOURNAL:16136829;WGROUP:STRING:PUBLICATION.

[76] G.-X. Liang *et al.*, "Self-powered broadband kesterite photodetector with ultrahigh specific detectivity for weak light applications," *SusMat*, vol. 3, no. 5, pp. 682–696, Oct. 2023, doi: 10.1002/SUS2.160.

[77] Y. Wang *et al.*, "Cauliflower-like copper zinc tin sulfur for ppb-level NO2 sensing at room temperature," *Sens. Actuators B Chem.*, vol. 393, p. 134212, Oct. 2023, doi: 10.1016/J.SNB.2023.134212.

[78] G. K. Dalapati *et al.*, "Impact of molybdenum out diffusion and interface quality on the performance of sputter grown CZTS based solar cells," *Scientific Reports 2017 7:1*, vol. 7, no. 1, pp. 1–12, May 2017, doi: 10.1038/s41598-017-01605-7.

[79] V. Pakštas *et al.*, "Improvement of CZTSSe film quality and superstrate solar cell performance through optimized post-deposition annealing," *Sci. Rep.*, vol. 12, no. 1, 2022, doi: 10.1038/s41598-022-20670-1.

[80] S. K. Kolekar *et al.*, "Synthesis and Characterization of CZTS Thin Films for Solar Cell Applications," *Innovations in Perovskite Solar Cell Materials and Devices - Cutting-Edge Research and Practical Applications*, Feb. 2025, doi: 10.5772/INTECHOPEN.1008712.

[81] S. Vangelista *et al.*, "Structural, chemical and optical properties of cerium dioxide film prepared by atomic layer deposition on TiN and Si substrates," *Thin Solid Films*, vol. 636, pp. 78–84, Aug. 2017, doi: 10.1016/J.TSF.2017.05.034.

[82] S. L. Chou, J. I. Lo, Y. C. Peng, H. C. Lu, B. M. Cheng, and J. F. Ogilvie, "Emission spectra of atomic and molecular nitrogen from photolysis of ammonia in solid neon," *AIP Adv.*, vol. 9, no. 5, p. 55311, May 2019, doi: 10.1063/1.5096280/1071359.

[83] M. Dragoman, A. Dinescu, F. Nastase, and D. Dragoman, "Memtransistors Based on Nanopatterned Graphene Ferroelectric Field-Effect Transistors," *Nanomaterials 2020, Vol. 10, Page 1404*, vol. 10, no. 7, p. 1404, Jul. 2020, doi: 10.3390/NANO10071404.

[84] A. Di Bartolomeo, F. Goubard, I. Boerasu, and B. Stefan Vasile, "Current Status of the Open-Circuit Voltage of Kesterite CZTS Absorber Layers for Photovoltaic Applications—Part I, a Review," *Materials 2022, Vol. 15, Page 8427*, vol. 15, no. 23, p. 8427, Nov. 2022, doi: 10.3390/MA15238427.

[85] E. Thimsen, S. C. Riha, S. V. Baryshev, A. B. F. Martinson, J. W. Elam, and M. J. Pellin, "Atomic layer deposition of the quaternary chalcogenide Cu2ZnSnS4," *Chemistry of Materials*, vol. 24, no. 16, pp. 3188–3196, Aug. 2012, doi: 10.1021/CM3015463/SUPPL_FILE/CM3015463_SI_001.PDF.

[86] M. Y. Zaki and A. Velea, "Recent Progress and Challenges in Controlling Secondary Phases in Kesterite CZT(S/Se) Thin Films: A Critical Review," *Energies 2024, Vol. 17, Page 1600*, vol. 17, no. 7, p. 1600, Mar. 2024, doi: 10.3390/EN17071600.

[87] H. Chen *et al.*, "Electrodeposited CZTS solar cells from Reline electrolyte," *Green Chemistry*, vol. 16, no. 8, pp. 3841–3845, Jul. 2014, doi: 10.1039/C4GC00142G.

[88] J. C. Lowe *et al.*, "Solution processed CZTS solar cells using amine–thiol systems: understanding the dissolution process and device fabrication," *J. Mater. Chem. C Mater.*, vol. 8, no. 30, pp. 10309–10318, Aug. 2020, doi: 10.1039/D0TC00955E.

[89] A. Krishnan, K. Rishad Ali, G. Vishnu, and P. Kannan, "Towards phase pure CZTS thin films by SILAR method with augmented Zn adsorption for photovoltaic applications," *Mater. Renew. Sustain. Energy*, vol. 8, no. 3, pp. 1–8, Sep. 2019, doi: 10.1007/S40243-019-0152-1/FIGURES/5.

[90] P. Aabel, A. Anupama, and M. C. Santhosh Kumar, "Preparation and characterization of CZTS thin films by vacuum-assisted spray pyrolysis and fabrication of Cd-free heterojunction solar cells," *Semicond. Sci. Technol.*, vol. 38, no. 4, p. 045010, 2023, doi: 10.1088/1361-6641/acbcea.

[91] A. Guchhait *et al.*, "Enhancement of Open-Circuit Voltage of Solution-Processed Cu2ZnSnS4 Solar Cells with 7.2% Efficiency by Incorporation of Silver," *ACS Energy Lett.*, vol. 1, no. 6, pp. 1256–1261, Dec. 2016, doi: 10.1021/ACSENERGYLETT.6B00509/ASSET/IMAGES/LARGE/NZ-2016-005099_0004.JPEG.

[92] J. B. Mooney and S. B. Radding, "SPRAY PYROLYSIS PROCESSING.," *Annual Review of Materials Science*, vol. 12, no. Volume 12, 1982, pp. 81–101, Aug. 1982, doi: 10.1146/ANNUREV.MS.12.080182.000501/CITE/REFWORKS.

[93] S. Huang, W. Luo, and Z. Zou, "Band positions and photoelectrochemical properties of Cu2ZnSnS4 thin films by the ultrasonic spray pyrolysis method," *J. Phys. D Appl. Phys.*, vol. 46, no. 23, p. 235108, May 2013, doi: 10.1088/0022-3727/46/23/235108.

[94] S. Agrawal, D. O. De Souza, C. Balasubramanian, and S. Mukherjee, "Effect of secondary phases controlled by precursor composition on the efficiency of CZTS thin film solar cell," *Solar Energy Materials and Solar Cells*, vol. 267, p. 112719, Apr. 2024, doi: 10.1016/J.SOLMAT.2024.112719.

[95] K. V. Gunavathy, C. Rangasami, A. M. S. Arulanantham, B. Felcia Merlin, C. Parthasaradhi Reddy, and A. Khan, "Enhancing the optoelectronic performance of CZTS thin films through cobalt doping via nebulizer-assisted spray pyrolysis technique," *Sens. Actuators A Phys.*, vol. 366, p. 114941, Feb. 2024, doi: 10.1016/J.SNA.2023.114941.

[96] M. Abbas *et al.*, "Highest Solar-to-Hydrogen Conversion Efficiency in Cu2ZnSnS4 Photocathodes and Its Directly Unbiased Solar Seawater Splitting," *Nanomicro Lett.*, vol. 17, no. 1, p. 257, 2025, doi: 10.1007/s40820-025-01755-8.

[97] D. Huang, K. Wang, L. Yu, T. H. Nguyen, S. Ikeda, and F. Jiang, "Over 1% Efficient Unbiased Stable Solar Water Splitting Based on a Sprayed $Cu_2ZnSnS_4$ Photocathode Protected by a $HfO_2$ Photocorrosion-Resistant Film," *ACS Energy Lett.*, vol. 3, no. 8, pp. 1875–1881, 2018, doi: 10.1021/acsenergylett.8b01005.

[98] S. Chamekh, N. Khemiri, and M. Kanzari, "Effect of annealing under different atmospheres of CZTS thin films as absorber layer for solar cell application," *SN Appl. Sci.*, vol. 2, no. 9, 2020, doi: 10.1007/s42452-020-03287-9.

[99] F. Jiang *et al.*, "Pt/$In_2S_3$/CdS/$Cu_2ZnSnS_4$ Thin Film as an Efficient and Stable Photocathode for Water Reduction under Sunlight Radiation," *J. Am. Chem. Soc.*, vol. 137, no. 42, pp. 13691–13697, 2015, doi: 10.1021/jacs.5b09015.